J. Fluid Mech. (2010), *vol.* 646, *pp.* 91–125.
doi:10.1017/S0022112009992813

Particle dynamics in a turbulent particle–gas suspension at high Stokes number. Part 2. The fluctuating-force model

PARTHA S. GOSWAMI AND V. KUMARAN†

Department of Chemical Engineering, Indian Institute of Science, Bangalore 560 012, India

(Received 20 December 2008; revised 14 October 2009; accepted 14 October 2009)

A fluctuating-force model is developed for representing the effect of the turbulent fluid velocity fluctuations on the particle phase in a turbulent gas–solid suspension in the limit of high Stokes number, where the particle relaxation time is large compared with the correlation time for the fluid velocity fluctuations. In the model, a fluctuating force is incorporated in the equation of motion for the particles, and the force distribution is assumed to be an anisotropic Gaussian white noise. It is shown that this is equivalent to incorporating a diffusion term in the Boltzmann equation for the particle velocity distribution functions. The variance of the force distribution, or equivalently the diffusion coefficient in the Boltzmann equation, is related to the time correlation functions for the fluid velocity fluctuations. The fluctuating-force model is applied to the specific case of a Couette flow of a turbulent particle–gas suspension, for which both the fluid and particle velocity distributions were evaluated using direct numerical simulations by Goswami & Kumaran (2010). It is found that the fluctuating-force simulation is able to quantitatively predict the concentration, mean velocity profiles and the mean square velocities, both at relatively low volume fractions, where the viscous relaxation time is small compared with the time between collisions, and at higher volume fractions, where the time between collisions is small compared with the viscous relaxation time. The simulations are also able to predict the velocity distributions in the centre of the Couette, even in cases in which the velocity distribution is very different from a Gaussian distribution.

1. Introduction

In the modelling of particulate phase of gas–solid suspensions with relatively large particles (i.e. of size greater than about 100 μm), it is necessary to deal with two complexities. The first is the complexity of the turbulent flow of the gas and the effect of the turbulent velocity fluctuations on the motion of particles. The second is the inertia of the particles themselves and the inter-particle interactions. If the particles are of relatively small size (1–3 μm), the particle Stokes number (ratio of particle inertia and fluid viscosity) is small. This implies that the particle relaxation time is small compared to the flow time scale, and so the the particles follow the motion of the local fluid streamlines. For larger particles of size about 100 μm, the particle Stokes number is large, though the Reynolds number (ratio of fluid inertia and viscosity) is relatively small, up to about 10. This implies that the drag force on the

† Email address for correspondence: kumaran@chemeng.iisc.ernet.in

particles is well approximated by the Stokes law or a modification of the Stokes law because of particle inertia. However, the high particle Stokes number implies that particles travel across streamlines because of their inertia and exert a force on the fluid. In addition, it is also necessary to incorporate, realistically, the direct collisional interactions between particles.

In the absence of significant fluid drag, the inertial flows of particles of size 100 μm and higher has been extensively studied in the context of granular flows. There has been much work on the derivation of constitutive relations for granular materials. Kinetic theory approaches make an analogy between the motion of the particles in a granular material and the motion of molecules in a gas and attempt to write down constitutive relations similar to those derived by the Chapman–Enskog procedure for hard-sphere gases (Chapman & Cowling 1970). There have been many formulations of the balance laws and constitutive relations for smooth inelastic particles (Savage & Jeffrey 1981; Jenkins & Savage 1983; Lun *et al.* 1984; Jenkins & Richman 1985). These models typically fall into two categories: the generalized Navier–Stokes equations, where the mass and momentum equations are similar to those for a simple fluid but where the energy equation has an additional term because of the dissipation of energy in inelastic collisions (Savage & Jeffrey 1981; Jenkins & Savage 1983; Lun *et al.* 1984; Sela, Goldhirsch & Noskowicz 1996; Sela & Goldhirsch 1998), and the moment expansion models (Jenkins & Richman 1985; Chou & Richman 1998), where the higher moments of the velocity distribution function are incorporated into the description. There have been derivations of kinetic equations up to Burnett order starting from the Boltzmann equation using an expansion with the Knudsen number and the inelasticity of the particle collisions as the small parameters (Sela *et al.* 1996; Sela & Goldhirsch 1998). A recent review (Goldhirsch 2003) concluded that hydrodynamic models have been unusually successful in describing rapid granular flows even though there is not a large-scale separation between the microscopic scale (particle diameter or mean free path) and the flow scales.

There has been less work on the effect of fluid velocity fluctuations on the flow of a granular material. Louge, Mastorakos & Jenkins (1991) studied the effect of particle collision in the turbulent suspension of a vertical pipe and considered the particulate phase as heavy dilute colliding grains, where the fluid exerts a drag force on the particles. In their case the source of particle fluctuation is inter-particle collision and not turbulent fluid velocity fluctuation. The effect of fluid drag on a particle–gas suspension has been studied for the case in which turbulent velocity fluctuations are not present for particles settling in a fluid (Kumaran & Koch 1993*a*, *b*) and for a shear flow (Tsao & Koch 1995). In addition, the effect of hydrodynamic interactions on the particle motion has been examined (Koch 1990). Kumaran (1998*b*) investigated the temperature scaling of the vibro-fluidized granular material in the limit in which the dissipation of energy because of inelastic collision or because of viscous drag between successive collisions is small compared with the energy of the particles and used the Boltzmann equation for the system which is identical to that for a gas at equilibrium in a gravitational field. Furthermore, Kumaran (1998*a*) introduced the correction to the distribution function because of dissipative effects, which was calculated using the moment expansion method. He found that the corrected density and temperature show qualitative agreement with the experimental results. In addition, Kumaran (2004) developed the constitutive relation for the granular flow of smooth, nearly elastic particles in the adiabatic limit, where the length scale for conduction is small compared with the macroscopic scale. He performed the linear stability analysis to investigate whether the Navier–Stokes approximation is capable of capturing

the leading behaviour of the growth rate in the small-wavenumber limit. Kumaran (2006*a*) also derived the constitutive relations for the granular flow of rough spheres in the limit in which the energy dissipation in a collision is small compared with the energy of a particle, using the perturbation expansion of the Boltzmann equation. He found the non-zero coefficient of bulk viscosity for rough and partially rough particles. The hydrodynamics of the dense granular flow of rough inelastic particles down an inclined plane was analysed by Kumaran (2008) using constitutive relations derived from kinetic theory. He introduced a fundamental length scale, 'conduction length', over which the rate of conduction of energy is comparable to the rate of dissipation. The effect of turbulent velocity fluctuations has been incorporated within the kinetic theory framework (Kumaran 2003) with the assumption that the effect of fluid velocity fluctuations can be modelled as Gaussian white noise, and the effect of these fluctuations on the stability of the linear shear flow of a granular material has been analysed. Here, we formulate a fluctuating-force description, where the effect of the fluid velocity fluctuations is incorporated as a Gaussian white noise on the particles. The noise statistics are obtained from the statistics of the fluid velocity fluctuations in the direct numerical simulation (DNS) by Goswami & Kumaran (2010). It was shown in part 1 that the statistics of the acceleration distribution on the particles is identical to that obtained from the fluid velocity fluctuations within the fluid. Therefore, we use the fluid velocity fluctuations in the absence of particles in the DNS to extract the force correlations in the fluctuating-force model. The results of the fluctuating-force model are then compared with the results of the DNSs with one-way coupling.

2. Theory

2.1. *Fokker–Plank description*

The Boltzmann equation for the particle velocity distribution function, for a two-dimensional flow with velocity in the x direction and velocity gradient in the y direction, can be expressed as

$$\frac{\partial f(\boldsymbol{v}')}{\partial t}+(\bar{v}_i+v_i')\frac{\partial f(\boldsymbol{v}')}{\partial x_i}-\dot{\gamma}\frac{\partial v_y' f(\boldsymbol{v}')}{\partial v_x'}-\frac{1}{\tau_v}\frac{\partial((v_i'+\bar{v}_i-\bar{u}_i)f(\boldsymbol{v}'))}{\partial v_i'}-\boldsymbol{D}_{ij}\frac{\partial^2 f(\boldsymbol{v}')}{\partial v_i'\partial v_j'}=\frac{\partial_c f(\boldsymbol{v}')}{\partial t}, \tag{2.1}$$

where $f(\boldsymbol{v}')$ is the particle velocity distribution function, defined such that $f(\boldsymbol{v}')\,\mathrm{d}\boldsymbol{v}'$ is the probability of finding a particle in the volume $d\boldsymbol{v}'$ about $\boldsymbol{v}'$ in the velocity space. Here, it is important to note that $\boldsymbol{v}'$ is the particle fluctuating velocity. The particle instantaneous velocity is $v_i'+\bar{v}_i$, where $\bar{v}_i(y)$ is the mean velocity in the streamwise direction, which is a function of the cross-stream coordinate y. The first term on the left-hand side of the (2.1) is the rate of change of distribution function with time; the second term is the rate of change of the distribution function because of particle motion; and the third term is the change in the distribution function because of mean shear on the particles, where $\dot{\gamma}=\mathrm{d}\bar{v}/\mathrm{d}y$ is the mean strain rate. The fourth term represents the effect of drag force on the particles, where τ_v is the viscous relaxation time of the particle. The fifth term is the change in distribution function because of fluctuating gas velocity modelled as Gaussian random noise. The term on the right-hand side of (2.1) is the rate of change of the distribution function because of particle collisions and is called the 'collision integral'. The collision integral can be

expressed as

$$\frac{\partial_c f(\boldsymbol{v}')}{\partial t} = \rho\chi(\phi)\int \mathrm{d}\boldsymbol{k}\int \mathrm{d}\boldsymbol{v}'^{*}\left(f(\boldsymbol{v}_b')f(\boldsymbol{v}_b'^{*}) - f(\boldsymbol{v}')f(\boldsymbol{v}'^{*})\right)\boldsymbol{w}\cdot\boldsymbol{k}. \tag{2.2}$$

In (2.2) $\boldsymbol{v}_b'$ and $\boldsymbol{v}_b'^{*}$ are the velocities of the pair of particles before the collision and $\boldsymbol{v}'$ and $\boldsymbol{v}'^{*}$ are the post-collisional velocities; $\boldsymbol{k}$ is the unit vector in the direction of the line joining centres of the colliding particles; $\boldsymbol{w} = \boldsymbol{v}' - \boldsymbol{v}'^{*}$ is the difference in velocity of the particles; $\chi(\phi)$ is the pair distribution function, which is 1 in the limit of low volume fractions analysed here. The integral in (2.2) is carried out for the condition $\boldsymbol{w}\cdot\boldsymbol{k} \geqslant 0$, so that the particles approach each other before the collision.

In a discrete particle simulation (event-driven simulations for example), the collision term is explicitly modelled in the form of instantaneous collisions between particles. The effect of the mean shear is also explicitly included because of the variation of the particle mean velocity with position. Therefore, it is necessary to modify the rules for particle advancement between collisions in order to include the effect of the random noise (representing the diffusivity in (2.1)) and the particle drag (which is the fourth term on the left-hand side of (2.1)). If the mean shear and collisions are neglected, then the Boltzmann equation (2.1) reduces to

$$\frac{\partial f(\boldsymbol{v}')}{\partial t} = \frac{1}{\tau_v}\frac{\partial(v_i' f(\boldsymbol{v}'))}{\partial v_i'} + \boldsymbol{D}_{ij}\frac{\partial^2 f(\boldsymbol{v}')}{\partial v_i'\partial v_j'}. \tag{2.3}$$

Equation (2.3) is equivalent to the Fokker–Planck equation, with the coefficient of diffusion in velocity space, $\boldsymbol{D}_{ij}$, given by

$$\boldsymbol{D}_{ij} = \int_0^\infty \mathrm{d}t'\langle a_i'(t')a_j'(0)\rangle = \frac{1}{\tau_v^2}\int_0^\infty \mathrm{d}t'\langle u_i'(t')u_j'(0)\rangle. \tag{2.4}$$

Here $\boldsymbol{a}'$ is the acceleration fluctuation, which is equal to $(\boldsymbol{u}'/\tau_v)$ if we only consider the acceleration because of the fluid velocity fluctuations and assume Stokes law. In (2.4), the implicit assumption is that the decay time for the fluid velocity fluctuations is small compared with the viscous relaxation time or the collision time, so that the effect of fluid velocity fluctuations can be accurately represented by Gaussian white noise. The diffusion tensor $\boldsymbol{D}_{ij}$ is a symmetric tensor and has dimensions of (length^2 time^{-3}). When the fluid is driven by the shear in the x–y plane, the components $\boldsymbol{D}_{xz}$ and $\boldsymbol{D}_{yz}$ are zero because the probability distribution for the velocity fluctuation in the z direction is an even function of u_z'.

The Langevin equation for a single particle, equivalent to (2.3), can be written as

$$\frac{\mathrm{d}\boldsymbol{v}}{\mathrm{d}t} = -\frac{(\boldsymbol{v}-\bar{\boldsymbol{u}})}{\tau_v} + \boldsymbol{F}(t). \tag{2.5}$$

The first term on the right-hand side of (2.5) is the drag of the particle because of the difference in the particle velocity and the fluid mean velocity. The second term is the fluctuating random force on the particle because of the fluid velocity fluctuations. The force $\boldsymbol{F}(t)$ is modelled as Gaussian white noise with zero mean and a second moment given by

$$\langle F_i(t)F_j(t)\rangle = 2\boldsymbol{D}_{ij}\delta(t-t'), \tag{2.6}$$

where $\boldsymbol{D}_{ij}$ is the diffusion coefficient, described in (2.3) and (3.1). It can easily be verified that with the second moments given in (2.6), the Langevin equation (2.5) is identical to the Fokker–Planck equation (2.3) for a homogeneous system. In the absence of collisions and mean shear, the particle and fluid phase mean velocities

are equal, since there is no net force acting on the particles. The solution for (2.3) or (2.5), with a force correlation given by (2.6), is a Gaussian distribution for the particle velocities, of the form

$$f = \frac{1}{(2\pi)^{3/2}\mathrm{Det}(\boldsymbol{T}_{ij})^{1/2}}\exp\left(-\frac{v_i' T_{ij}^{-1} v_j'}{2}\right), \tag{2.7}$$

where the 'temperature' tensor of the mean square velocities, $\boldsymbol{T}_{ij}$, is

$$\boldsymbol{T}_{ij} = \tau_v \boldsymbol{D}_{ij}. \tag{2.8}$$

In the presence of a mean shear and particle collisions, the Langevin equation (2.5) still applies between successive particle collisions, provided we use the local mean velocity of the particle in the drag term.

Therefore, the equation for particle motion between collisions is modified as,

$$\frac{\mathrm{d}v_i}{\mathrm{d}t} = -\frac{v_i - \bar{u}_i(\boldsymbol{x}_p)}{\tau_v} + F_i(t). \tag{2.9}$$

where $\bar{u}_i(\boldsymbol{x}_p)$ is the mean velocity at the local particle position. This is combined with instantaneous collisions when two particles come in contact using the collision laws for spherical elastic particles, to obtain a 'fluctuating-force' simulation procedure for the particle phase.

The value of the random force $\boldsymbol{F}$ has to be chosen with care so that it is in agreement with the second-moment equation (2.6). We consider a small time period Δt, for which the differential equation (2.9) can be approximated as a difference equation,

$$v_i(t+\Delta t) - v_i(t) = -\frac{(v_i - \bar{u}_i)\Delta t}{\tau_v} + F_i \Delta t \tag{2.10}$$

where F_i is a stochastic force which has to be generated in accordance with (2.6). The force magnitudes cannot be generated in the usual manner used for isotropic Gaussian noise because the off-diagonal component $\boldsymbol{D}_{xy}$ of the diffusion matrix in (2.6) is non-zero. The magnitude of the force is determined by generating three independent normal random deviates, namely ζ_1, ζ_2 and ζ_3, with zero mean and unit variance. The components of the force, F_i, are then expressed as

$$\left.\begin{aligned} F_x &= \frac{\sqrt{2\boldsymbol{D}_{xx}}\zeta_1}{\sqrt{\Delta t}}, \\ F_y &= \frac{\sqrt{2\boldsymbol{D}_{yy}}}{\sqrt{\Delta t}}\left(\frac{\boldsymbol{D}_{xy}\zeta_1}{\sqrt{\boldsymbol{D}_{xx}\boldsymbol{D}_{yy}}} + \zeta_2\sqrt{1 - \frac{\boldsymbol{D}_{xy}^2}{\boldsymbol{D}_{xx}\boldsymbol{D}_{yy}}}\right), \\ F_z &= \frac{\sqrt{2\boldsymbol{D}_{zz}}\zeta_3}{\sqrt{\Delta t}}. \end{aligned}\right\} \tag{2.11}$$

It can be easily verified that the above choice provides the correct second moment of the force distribution as required in (2.6), appropriate for a finite-difference formulation, with $\delta(t-t')$ replaced by $(1/\Delta t)$.

In case a collision occurs within the time of advance Δt, the particle velocity is changed in accordance with the collision rule, but the particle acceleration is unchanged for the entire time period Δt. At every time step, the particle acceleration

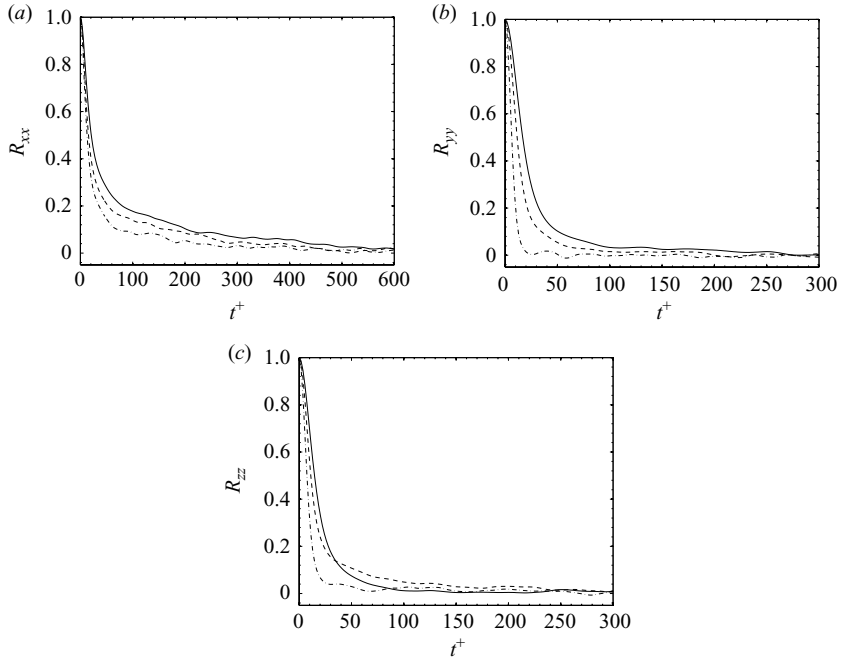

FIGURE 1. Eulerian time correlation of the streamwise fluid velocity fluctuation at different cross-stream positions: $y^+ = 2.2$ (–.–), $y^+ = 26.4$ (––), $y^+ = 46.8$ (—) for (*a*) streamwise fluid velocity fluctuation, (*b*) wall-normal fluid velocity fluctuation and (*c*) spanwise fluid velocity fluctuation.

from the drag force and the random forcing are calculated. Using this acceleration and the particle velocity and position, we predict the collision time. If collision occurs during Δt, we modify the velocity according to collision rule, and consequently the acceleration because of drag changes, but we use the same acceleration owing to random forcing (fluctuating force) in the rest of the time step.

3. Simulation technique

The configuration and coordinate system is the same as we have used in the DNS (figure 1) in Goswami & Kumaran (2010). The fluctuating-force simulations have been carried out using a variable-time-step molecular dynamics procedure, and the time step for advancement is less than the integral time scale of the fluid. As mentioned before, we are interested in the regime for which the viscous relaxation time and the collision time of the particles are larger than the integral fluid time scale. The second moment of the random force in the simulations is determined from the autocorrelation function of the fluid velocity fluctuations in a Eulerian reference frame, since it was found in part 1 of the present paper (Goswami & Kumaran 2010) that the distribution function for the particle acceleration because of the fluid velocity fluctuations can be obtained from the distribution of the fluid velocity fluctuations in a Eulerian reference frame. It should be noted that the fluid velocity fluctuations are position dependent, and they vary in the wall-normal direction. Therefore, the second moment of the distribution of the random force is also a function of position. We start our simulation with random initial configuration of the particles. At each step, we need to calculate the fluid drag on the particle, which is generated because of

the difference in particle instantaneous velocity and the local average fluid velocity; the latter is obtained from the results of the DNS of Couette flow in the absence of the particles Goswami & Kumaran (2010). We use cubic spline interpolation in the wall-normal direction to obtain the average fluid velocity at the the particle position.

Particle collisions are implemented using the usual collision rules between spherical elastic particles, where the relative velocity along the line joining the centres of the particles is reversed in a collision, while the relative velocity perpendicular to the line joining the centres remains unchanged. Impending particle collisions are predicted in a deterministic method, as done in case of the DNS, and not using the type of stochastic procedure used in direct simulation Monte Carlo. We consider only the binary collision because the probability of multi-body collision is small at low volume fractions. To make the collision prediction more computationally efficient, we divide the simulation domain in three-dimensional lattice cells, and then we find the collision time for each particle by scanning potential collision partners from the same cell or from the neighbouring cells. We have used 15^3 lattice cell with average two to three particle per cell. The updating of the particle velocity is done according to (2.10), with the random noise chosen in accordance with (2.11). At every step we need to calculate the drag on the particle which depends on its wall-normal position. If a collision occurs within the simulation time step Δt, we advance all the particles in position and velocities by the time Δt_c up to the collision time. The post-collisional velocities of the colliding particles are calculated by (2.10) in part 1 of the current work (Goswami & Kumaran 2010), and the simulation is advanced further until the end of the time step.

Next, we turn to the issue of obtaining the elements of the diffusion tensor, $\boldsymbol{D}_{ij}$ from the DNSs of the fluid phase. As the results of part 1 (Goswami & Kumaran 2010) have indicated, the acceleration distribution on the particles because of the fluid velocity fluctuations can be accurately captured from the distribution of fluid velocity fluctuations in a Eulerian reference frame within the fluid. Therefore, in order to obtain the components of $\boldsymbol{D}_{ij}$, we determine the autocorrelations of the fluid velocity fluctuations in the fluid. However, it is important to note that the Eulerian time correlation function is a function of position along the wall-normal direction, and it is necessary to calculate the autocorrelation function at each position in the wall-normal direction.

The second moments for the random force distributions (2.6) are calculated from the velocity autocorrelation function for the fluid fluctuating velocity in a Eulerian reference frame in the absence of the particles and using equation (3.1):

$$\boldsymbol{D}_{ij} = \frac{\langle u_i'(0)u_j'(0)\rangle}{\tau_v^2}\int_0^\infty \mathrm{d}t' \frac{\langle u_i'(t')u_j'(0)\rangle}{\langle u_i'(0)u_j'(0)\rangle} = \frac{\langle u_i'(0)u_j'(0)\rangle}{\tau_v^2}\int_0^\infty \mathrm{d}t' \boldsymbol{R}_{ij}, \tag{3.1}$$

where $\boldsymbol{R}_{ij}$ is the Eulerian time correlation tensor of turbulent flow field. From the DNS, we can calculate the Eulerian time correlation function. Figures 1(a)–1(c) show the decay of the x, y and z components of the correlation function at different wall-normal positions of the Couette. To calculate the correlation functions from the DNS we have used larger box size than that used in part 1 (Goswami & Kumaran 2010) to allow the long tail of the correlation (mainly for streamwise fluid velocity fluctuation) to decay to zero, mimicking the infinite-box-length assumptions. The size of the box used in this case was $28\pi\delta \times 2\delta \times 8\pi\delta$, where δ is the channel half-width and the upper limit of time for integration used as 600 wall units. The non-zero

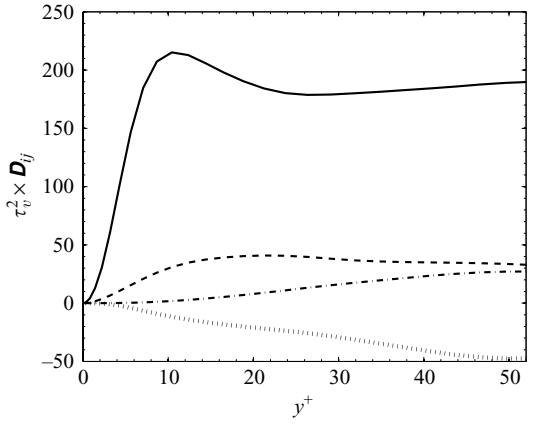

FIGURE 2. Velocity space diffusion coefficient across the width of the Couette: $\boldsymbol{D}_{xx}$ (—), $\boldsymbol{D}_{yy}$ (—.—), $\boldsymbol{D}_{zz}$ (——), $\boldsymbol{D}_{xy}$ (· · ·).

components of diffusion tensor, obtained using (3.1), have been shown as a function of the wall-normal coordinate in figure 2.

3.1. *Validation of the simulation code*

To validate our simulation code, we consider a system with no mean fluid velocity and no spatial variations, and we assume that the particles do not undergo collisions. The diffusion tensor is assumed to be anisotropic with a non-zero value of $\boldsymbol{D}_{xy}$, as appropriate for a shear flow. In this case, the system is described by the Langevin equation (2.5) with zero mean velocity, and the distribution of particle velocities should be given by (2.7) and (2.8). Therefore, our code validation consists of carrying out the 'fluctuating-force' simulations to test whether the probability distribution of the particle velocities is Gaussian and whether the velocity variances are consistent with (2.7) and (2.8). We have carried out this validation using the magnitude of the diffusion tensor as τ_v^2 times $\boldsymbol{D}_{xx} = 210.34$, $\boldsymbol{D}_{yy} = 4.46$, $\boldsymbol{D}_{zz} = 31.51$ and $\boldsymbol{D}_{xy} = -17.40$. The results show that the distribution of particle velocities is a Gaussian distribution in all three directions; we do not provide the details here for brevity. We have compared the mean square of the fluctuating particle velocity obtained by simulation with the results obtained theoretically from (2.8). Figures 3(*a*)–3(*c*), show the quantitative agreement of the different components of the particle mean square velocities for a wide range of the particle relaxation time.

4. Results of the fluctuating-force simulation

The results of the fluctuating-force simulations, formulated as discussed above, are compared with the results of the DNS for a range of ratios of the viscous relaxation time and time between collisions. Table 1 shows the parameter values for which we have carried out the DNSs. The number of particles in the simulations has been restricted to 8000, in order to reduce computation time. Because of this, the ratio of the channel width to particle diameter is relatively small at fixed volume fraction, as shown in table 1. We have assumed that the particle diameter is 39 μm for calculating the viscous relaxation time in order to make a connection to real flows, and because of this, the channel thickness has a maximum value of about 4 mm. It would be desirable to simulate a channel thickness of about 4 cm in order to make

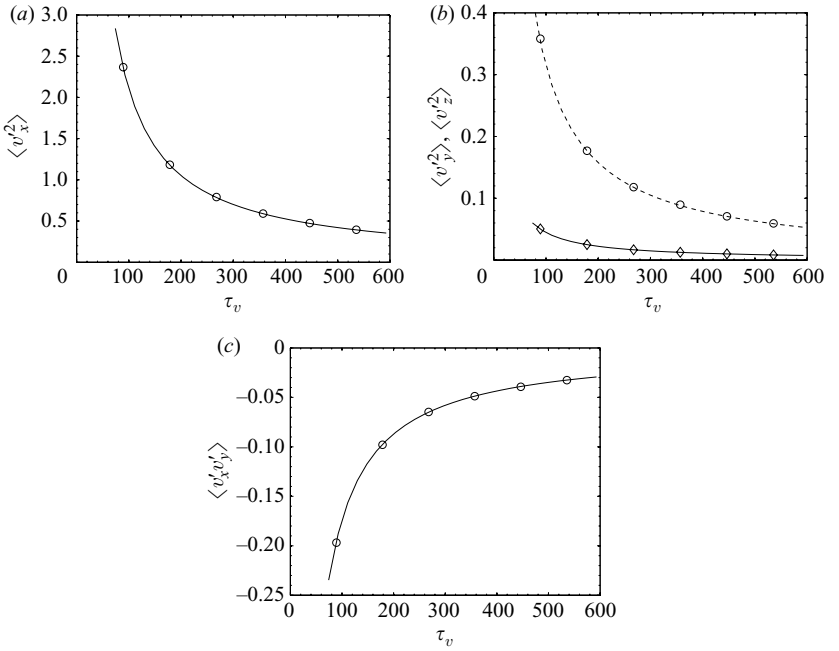

FIGURE 3. Comparison of the particle velocity fluctuation obtained from theory (—) and fluctuating-force simulation (○) with different viscous relaxation times of the particle: (*a*) $\langle v_x'^2 \rangle$, theory (—) and simulation (○); (*b*) $\langle v_y'^2 \rangle$, theory (—) and simulation (◇); $\langle v_z'^2 \rangle$, theory (——) and simulation (○); (*c*) $\langle v_x' v_y' \rangle$, theory (—) and simulation (○).

the simulations relevant for real applications, but this would require increasing the number of particles by a factor of 10^3, which would make it unfeasible to probe the large range of parameters we have been able to access, as shown in table 1. We have restricted the particle number so that in both the DNS and the fluctuating-force formulations, we are able to obtain profiles for all the particle concentrations, velocities and fluctuating velocities across the entire channel over a range of parameters. The viscous relaxation time has been varied independently by changing the mass density of the particles. The average time between collisions has been obtained by counting the total number of collisions in the simulation and dividing by the period of the simulation. Since the channel width is small, particles sometimes travel from one wall to the other without colliding with another particles. Therefore, we have also independently calculated the average time between particle–particle collisions and particle–wall collisions. The Stokes number in the present case is also reported as the ratio of the viscous relaxation time of the particle to the integral time scale of the fluid. All length and velocity scales are reported in dimensionless form, and they are non-dimensionalized by the friction length and the friction velocity.

Since the effect of the fluid velocity fluctuations is modelled as a random force which is a delta function in time, the assumption is that the correlation time of the turbulent velocity fluctuations τ_f is small compared with all other time scales in the problem, including the viscous relaxation time (τ_v), the time between particle collisions ($\tau_{c_{pp}}$) and the time between collisions with the wall ($\tau_{c_{pw}}$). The ratio (τ_v/τ_f), shown explicitly in table 1, is always larger than 1 and varies in the range 4–40. Since $\tau_{c_{pw}}$ is lower than $\tau_{c_{pp}}$ in most cases, it is also of interest to examine whether the

Number of particles (N_p)	Simulation runs	Particle density (ρ_p)	Solid volume fraction (ϕ_s)	$2\delta/d_p$	Relaxation time of the particle (τ_v)	Particle–particle collision time ($\tau_{c_{pp}}$)	Particle–wall collision time ($\tau_{c_{pw}}$)	Particle Stokes number ($St = \tau_v/\tau_f$)
(a) Viscous relaxation time of the particle is less than the particle–particle collision time. ($\tau_v < \tau_{c_{pp}}$)								
	1	2500			223.2	760.5	294.5	4.1
	2	3000			267.8	802.1	293.6	4.9
8000	3	4000	9.44×10^{-5}	76.6	357.1	869.8	295.1	6.6
	4	5000			446.4	998.0	300.2	8.2
	5	6000			535.7	1022.5	306.7	9.9
(b) Viscous relaxation time of the particle is less than the particle–wall collision time. ($\tau_v < \tau_{c_{pw}}$)								
	6	4000			193.9	2404.2	416.7	3.6
4000	7	5000	1.9×10^{-5}	103.97	242.4	2585.9	410.8	4.5
	8	6000			290.8	2712.0	405.1	5.4
	9	7000			339.3	2779.9	413.5	6.3
(c) Particle–particle collision time is less than the viscous relaxation time of the particle. ($\tau_{c_{pp}} < \tau_v$)								
	10	1500			509.3	340.9	244.5	9.4
	11	2000			679.0	351.0	248.8	12.6
	12	2500			848.8	386.3	255.4	15.7
8000	13	3000	7.0×10^{-4}	39.3	1018.5	419.0	263.2	18.8
	14	4000			1358.0	480.4	285.0	25.1
	15	5000			1697.5	493.5	291.5	31.4
	16	6000			2037.0	541.8	309.7	37.6

TABLE 1. The particle–particle and particle–wall collision time for particles with different relaxation times and with different solid volume fractions, $Re = 750$, based on half of the channel width and half of the difference between the velocities of the wall.

ratio ($\tau_{c_{pw}}/\tau_f$), is small. It can easily be verified for runs 10–16 that with the lowest values of $\tau_{c_{pw}}$, the ratio ($\tau_{c_{pw}}/\tau_f$) varies between 4.5 and 6, indicating that the time between particle-wall collisions is also large compared with the integral time in all cases. Therefore, all simulations are in the regime in which the integral time is small compared with all other time scales in the problem.

There are three different types of comparisons made in the simulations. The first is a comparison of the concentration profiles, the mean velocity profiles and the root mean square fluctuation velocities of the particles across the width of the channel. This comparison provides an indication of the variation in the dynamical quantities across the channel for given values of the collision time and the viscous relaxation time. A second comparison made is the variation of the the mean square velocities in the central 20 % of the channel as a function of the ratios of the viscous relaxation time to the fluid time scale. One of the important assumptions made in the fluctuating-force formulation is that the viscous relaxation time is large compared with the integral time scale for the fluid velocity fluctuations. If the viscous relaxation time is comparable to the integral time scale, then the formulation will not provide accurate results. The comparison of the mean square velocities with viscous relaxation time is intended to test this assumption and to provide some indication of the range of ratios of the viscous relaxation time and integral time for which the fluctuating-force formulation

provides accurate results. In addition, in our comparison of root mean square velocity profiles, we use a viscous relaxation time at the lower end of the range that we have studied, which is only about four times the integral time scale. This is intended to make a comparison under the most stringent conditions, in which the Gaussian white noise approximation for the fluctuating-force is expected to be the least valid.

The third is a comparison of the velocity distributions from the fluctuating-force simulations and the DNSs. An issue of interest is the form of the velocity distributions. It was shown, in part 1 (Goswami & Kumaran 2010), that though the acceleration distribution functions are always near Gaussian, the fluid velocity distributions in the wall-normal and spanwise directions deviate significantly from a Gaussian distribution. It is necessary to examine whether the fluctuating-force simulations also predict a similar form for the particle velocity distribution.

The comparisons have been made in three volume fraction regimes. The first is the volume fraction regime in which the viscous relaxation time is small compared with the particle–particle collision time, but the particle–wall collision time is of the same magnitude as the relaxation time. In this regime, designated as the free-flight regime, the particle will collide with the wall before relaxing. The second is at very low volume fraction, where the viscous relaxation time is small compared with both the particle–particle and the particle–wall collision time. The third is in the regime in which the collision time is small compared with the viscous relaxation time. For each set, we run the simulation for a time period that is three to five times τ_v, required for the steady state to be achieved. Then we start the sampling for a duration of three times τ_v.

In the results reported here, we have non-dimensionalized the variables based on the wall units, similar to the case of the DNS described in part 1 (Goswami & Kumaran 2010). The units of length and time are ν/u_* and ν/u_*^2, where ν and u_* are the kinematic viscosity and the friction velocity of the particle-free carrier phase. The friction velocity is defined as $u_* = (\tau_w/\rho)^{1/2}$, where τ_w is the wall shear stress. The size of our computational domain is $10\pi\delta \times 2\delta \times 4\pi\delta$, where δ is the channel half-width. For all the simulations, the carrier phase is air at ambient condition, and the simulation is done at isothermal condition. Based on the friction velocity the fluid phase Reynolds number $Re_\tau = 52.7$; the wall velocity is 14.2; and the shear rate is 3.71. The error bars reported in the DNS results have been calculated over the average of 20 ensembles of 1000 samples each.

4.1. *Viscous relaxation time is less than the particle–particle collision*

First, we consider the flow for a volume fraction of 9.44×10^{-5}, where the viscous relaxation time is small compared to the time between collisions. The particle–wall collision time is either of the same order or smaller than the particle relaxation time. The particle relaxation time and the time period for the collisions are reported in table 1.

In this case, the particle fluctuations are driven by both the fluctuating force and the inter-particle collisions, and there is a damping effect because of the drag force on the particles. To study the effect of particle inertia, we have changed the particle density which in turn changes the particle relaxation time, as was done in part 1.

Figure 4 shows the mean streamwise particle velocities at different wall-normal positions of the Couette for two different values of the particle relaxation time. The variation in the normalized particle concentration is shown in figure 5, where the normalization has been done with respect to the initial homogeneous particle concentration. The mean velocity profile for the particles shows a substantial slip

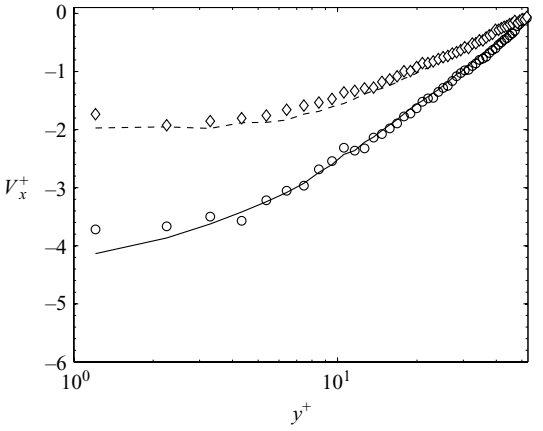

FIGURE 4. Variation of the streamwise particle velocity in the wall-normal direction for different particle relaxation times. In all the cases the viscous relaxation time of the particle is less than the particle–particle collision time ($\tau_v < \tau_{c_{pp}}$) and $\phi = 9.44 \times 10^{-5}$. Simulation: run 2, DNS (○); run 5, DNS (◇); run 2, FFS (—); run 5, FFS (——). The parameters for all the runs are given in table 1.

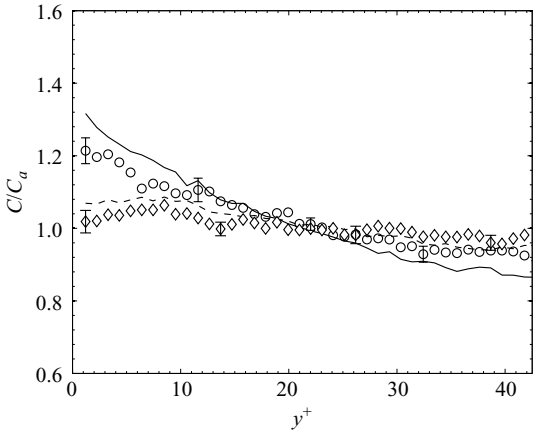

FIGURE 5. Variation of the normalized particle concentration. The viscous relaxation time of the particle is less than the particle–particle collision time ($\tau_v < \tau_{c_{pp}}$) and $\phi = 9.44 \times 10^{-5}$. Simulation: run 2 , DNS (○); run 5, DNS (◇); run 2, FFS (—); run 5, FFS (——). The parameters for all the runs are given in table 1.

at the wall, as the wall velocity is 14.2 times the friction velocity. The particle concentration profile shows that there is a migration of the particles towards the wall of the channel at lower particle relaxation time; this is because of the inhomogeneity in the fluctuating force exerted on the particles. Since the mean square of the fluctuating force (because of the fluid velocity fluctuations) is larger at the centre of the channel, a diffusion of particles towards the wall is caused. In both cases, it is observed that there is quantitative agreement between the DNS and the fluctuating-force simulations, even though the viscous relaxation time is only about five times the fluid integral time scale for the lower value of the particle relaxation time in the fluctuating-force simulations.

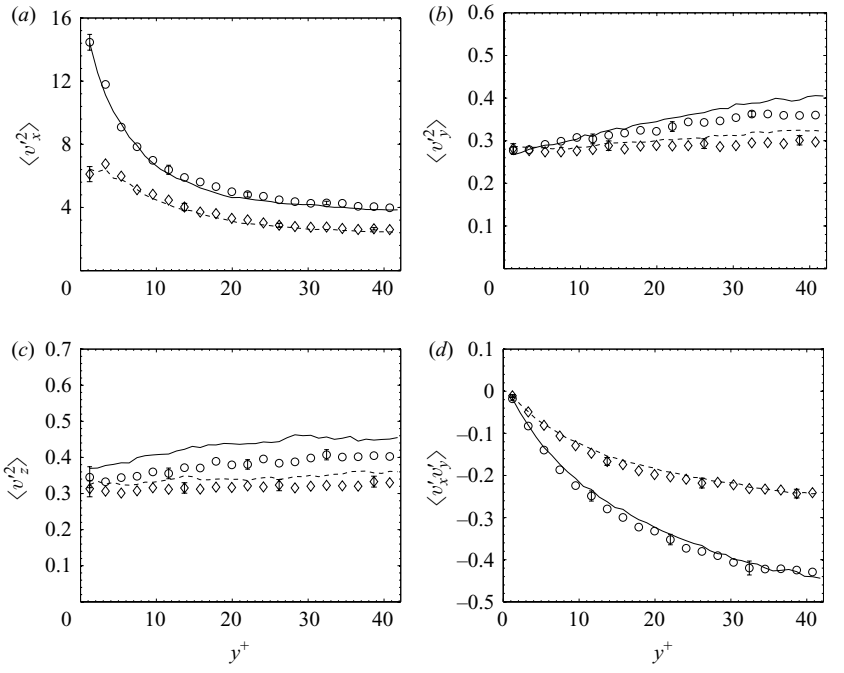

FIGURE 6. Second moments of the particle velocity distribution (*a*) $\langle v_x'^2 \rangle$, (*b*) $\langle v_y'^2 \rangle$, (*c*) $\langle v_z'^2 \rangle$ and (*d*) $\langle v_x' v_y' \rangle$ at different cross-stream positions. In all the cases the viscous relaxation time of the particle is less than the particle–particle collision time ($\tau_v < \tau_{c_{pp}}$) and $\phi = 9.44 \times 10^{-5}$. Simulation: run 2, DNS (○); run 5, DNS (◇); run 2, FFS (—); run 5, FFS (——). The parameters for all the runs are given in table 1.

Figure 6 shows the variation of the second moments of the particle velocity distributions with the cross-stream distance. It is found that the mean square velocities in the flow direction are quantitatively predicted by the fluctuating-force simulations. The streamwise mean square velocities increase as the wall is approached for two reasons. The first is that the increase in the velocity gradient as the wall is approached, which results in greater fluctuations because of the cross-stream motion of the particles. The second is that the mean square of the fluid velocity fluctuations also shows a maximum near the wall of the channel, as shown in figure 3 of part 1 (Goswami & Kumaran (2010). It should be noted that the particle–wall collisions are considered to be elastic and smooth, so that they do not result in fluctuations along the streamwise direction. The second moment of the velocity distribution $\langle v_x' v_y' \rangle$ is also quantitatively predicted by the fluctuating-force simulations. The moment $\langle v_x' v_y' \rangle$ is the particle-phase streaming stress. This stress has to go to zero at the wall for the particle–wall collision model we have chosen, because particle–wall collisions are elastic and smooth, and they do not exert any net stress on the particles. The mean square velocities in the wall-normal and spanwise directions are also in good agreement, though the difference is larger than that in the streamwise direction. It should be noted that the mean square velocities in these directions are small compared with those in the streamwise direction in both the DNS and the fluctuating-force simulations.

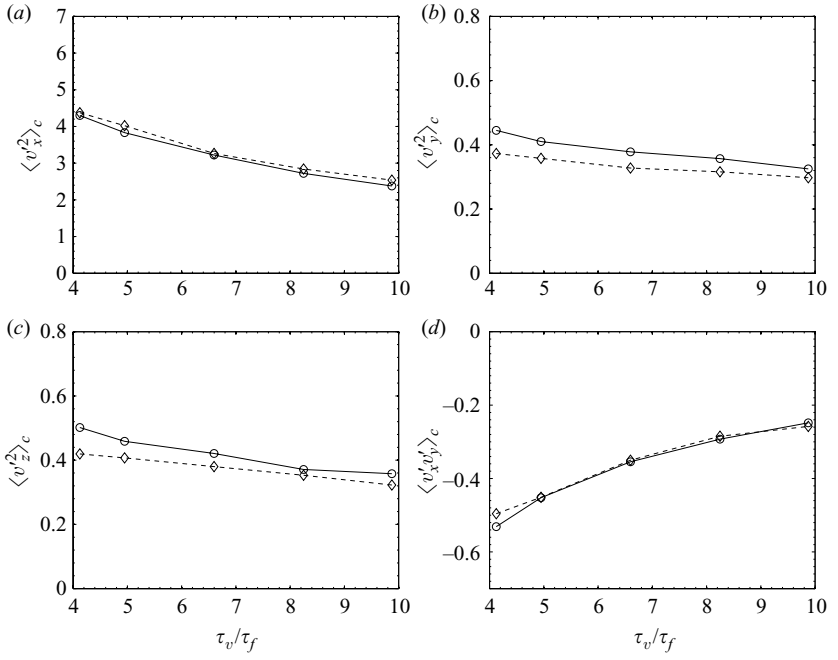

FIGURE 7. Second moments of the particle velocity distribution (*a*) $\langle v_x'^2\rangle$, (*b*) $\langle v_y'^2\rangle$, (*c*) $\langle v_z'^2\rangle$ and (*d*) $\langle v_x'v_y'\rangle$ obtained from the DNS (– – ◇) and the FFS (—○), averaged over the homogeneous centre core of the Couette. The viscous relaxation time of the particle is less than the particle–particle collision time, ($\tau_v < \tau_{c_{pp}}$) and $\phi = 9.44 \times 10^{-5}$. Simulation from run 1 to run 5. The detailed parameters for all the runs are given in table 1.

Figure 7 shows the second moments of the velocity distribution averaged over the central 20 % of the Couette ($y/\delta = 0.8$ to 1.2), where the root mean square of the fluid velocity is nearly a constant, as a function of the ratio of the viscous relaxation time and the fluid integral time scale (τ_v/τ_f). The integral time scale assumed here is that for velocity fluctuations in the streamwise direction, since this is larger than that in the wall-normal and spanwise directions. There is excellent agreement between the fluctuating force and the DNS for the root mean square velocities in the streamwise direction and in the second moment $\langle v_x'v_y'\rangle$. As expected, the agreement becomes better as the ratio (τ_v/τ_f) increases. The comparison for the mean square velocities in the wall-normal and spanwise directions are also well predicted by the fluctuating-force simulations, though the agreement is not as good as that for the streamwise mean square velocity.

The velocity distribution functions for the for the case ($\tau_v < \tau_{c_{pp}}$) are shown as the function of the particle fluctuating velocity in figure 8. The distribution functions have been calculated in the central 20 % of the Couette, where the fluid root mean square velocities are nearly a constant. The first important results of this comparison is that the fluctuating force is able to quantitatively capture the distribution of the particle velocities and not just the moments of the velocity distribution. The second important result is that the fluctuating-force simulation accurately captures the non-Gaussian nature of the velocity distribution in the wall-normal and the spanwise direction that is observed in the DNSs. The agreement in all cases is quantitative up to about three decades of variation in the distribution function.

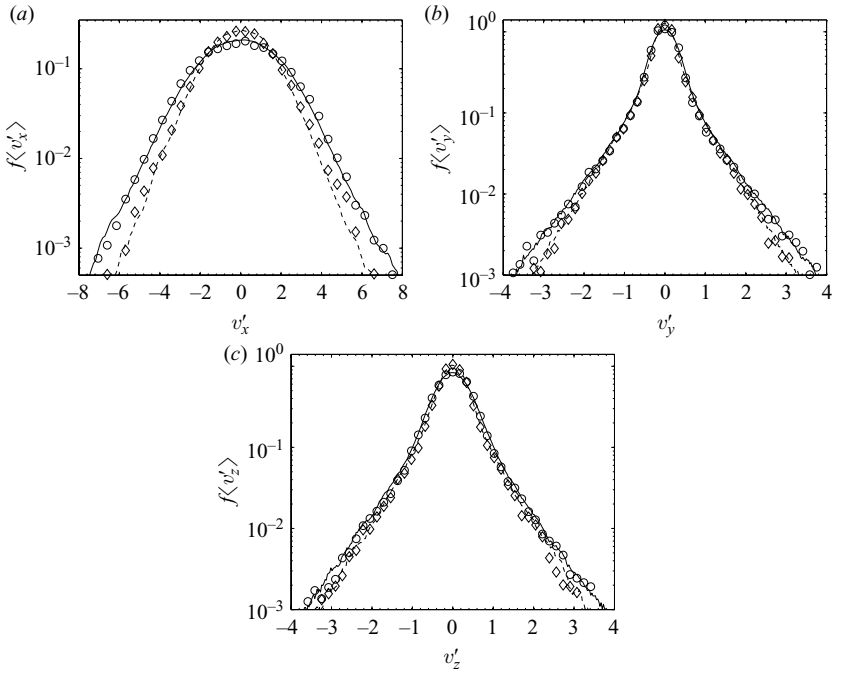

FIGURE 8. The particle velocity distribution function at the centre core of the Couette for the (*a*) streamwise, (*b*) wall-normal and (*c*) spanwise components of velocity fluctuations. The viscous relaxation time of the particle is less than the particle–particle collision time ($\tau_v < \tau_{c_{pp}}$) and $\phi = 9.44 \times 10^{-5}$. Simulation: run 2, DNS (○); run 5, DNS (◇); run 2, FFS (—); run 5, FFS (——). The parameters for all the runs are given in table 1.

4.2. *Viscous relaxation time is less than the particle–wall collision time*

In this section we concentrate on the dilute regime with solid volume fraction 1.9×10^{-5}, where the relaxation time is less than both the particle–particle and the particle–wall collision time. The particle relaxation and the collision times are reported in table 1. Figure 9 shows the mean streamwise particle velocity across the width of the Couette for different particle relaxation times. The figure clearly indicates that at higher values of y^+ near the centre of the Couette, the prediction from both the simulations matches very well. Near the wall there is a maximum difference that is within 15 %. In this case, the low particle Stokes number (4–5) might be the reason of the deviation. The normalized particle concentration is shown in figure 10. Because of the higher values of fluid fluctuating velocities at the centre, particles migrates towards the wall. The near-wall particle concentration is nearly two times the centre-plane concentration. The concentration profile obtained from the fluctuating-force simulation matches fairly well with the results of the fluctuating-force simulation, except very near the wall region and for the particle with very low relaxation time.

Figure 11 shows the variation of the second moment of the particle velocity fluctuation at different cross-stream positions for the particles with different viscous relaxation times. The magnitude of second moment decreases with increasing particle relaxation time. Results obtained from the fluctuating-force simulation matches well with the DNS results for streamwise fluctuation. Figures 11(*a*) and 11(*b*) show the variation of the wall-normal and spanwise velocity fluctuations at different cross-stream positions. The fluctuating-force simulation overpredicts the second moment

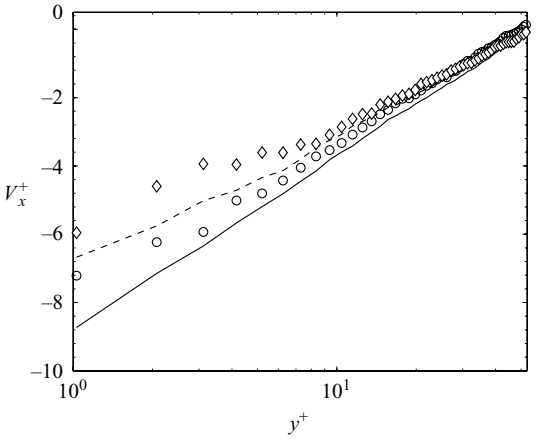

FIGURE 9. Variation of streamwise particle velocity in the wall-normal direction. The viscous relaxation time of the particle is less than the particle–wall collision time ($\tau_v < \tau_{c_{pw}}$) and $\phi = 1.9 \times 10^{-5}$. Simulation: run 7, DNS (○); run 9, DNS (◇); run 7, FFS (—); run 9, FFS (——). The parameters for all the runs are given in table 1.

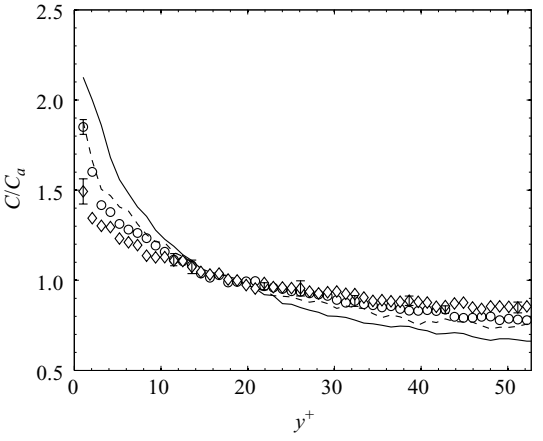

FIGURE 10. Variation of the normalized particle concentration. The viscous relaxation time of the particle is less than the particle–wall collision time ($\tau_v < \tau_{c_{pw}}$) and $\phi = 1.9 \times 10^{-5}$. Simulation: run 7, DNS (○); run 9, DNS (◇); run 7, FFS (—); run 9, FFS (——). The parameters for all the runs are given in table 1.

of these two components by 15 % at the centre, though the near-wall stress is well predicted. Figure 11(*c*) shows the second moment $\langle v_x' v_y' \rangle$ at different y^+. As we move towards the centre the magnitude of the shear stress increases. The near-wall particle shear stress is zero. The fluctuating-force simulation prediction shows good agreement with the results from the DNS.

Figure 12 shows the second moment of the particle velocities averaged over the central 20 % of the Couette. There is good agreement between the fluctuating force and the DNS for the root mean square velocities in the streamwise direction. In the wall-normal and spanwise directions differences between the results predicted by two simulation technique are 15–20 %. The figure shows the decrease in the second moment of particle velocity $\langle v_x' v_y' \rangle$ with increasing particle inertia. In this case also

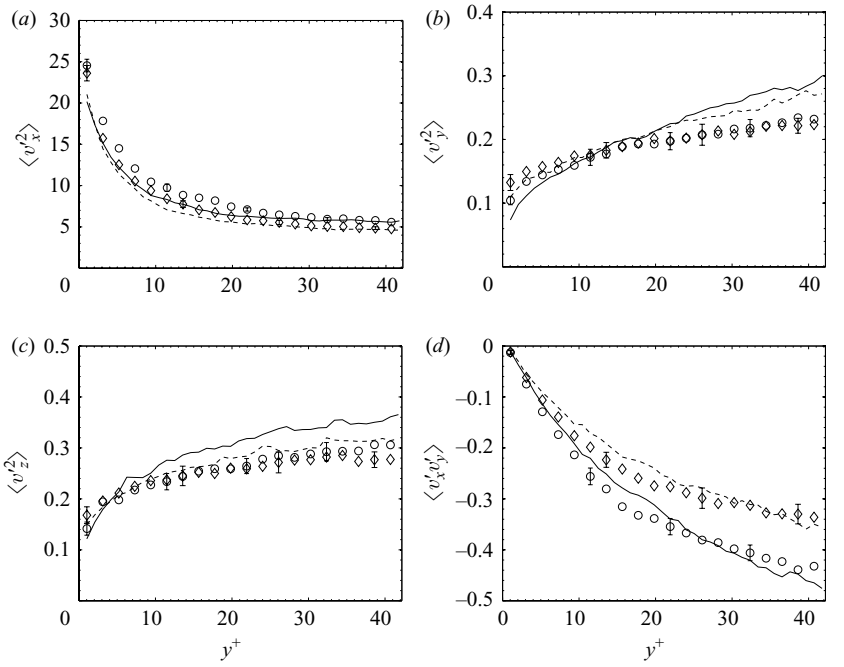

FIGURE 11. Variation of the second moments of the particle velocity distribution (*a*) $\langle v_x'^2 \rangle$, (*b*) $\langle v_y'^2 \rangle$, (*c*) $\langle v_z'^2 \rangle$ and (*d*) $\langle v_x' v_y' \rangle$ at different cross-stream positions. In all cases viscous relaxation time of the particle is less than the particle–wall collision time ($\tau_v < \tau_{c_{pw}}$) and $\phi = 1.9 \times 10^{-5}$. Simulation: run 7, DNS (○); run 9, DNS (◇); run 7, FFS (—); run 9, FFS (——). The parameters for all the runs are given in table 1.

results of the fluctuating-force simulations are in good agreement with the DNS results.

The particle velocity distribution function for both the simulations are shown in figure 13. As in the previous cases the distribution functions have been calculated at the central 20 % of the Couette. For the clarity of the figures, we have not plotted the corresponding Gaussian distributions. The streamwise velocity distribution obtained from the fluctuating-force simulation fits well with that obtained from the DNS. In addition, the fluctuating-force simulations capture the non-Gaussian nature of the velocity distribution in the wall-normal and the spanwise direction that is observed in the DNS.

4.3. *Particle–particle collision time is less than the viscous relaxation time*

Next, we consider the case in which the inter-particle collision time is less than the viscous relaxation time at a solid volume fraction of 7×10^{-4}. Table 1 gives the particle relaxation times and the collision times for the particle–particle and particle–wall collisions. Figure 14 shows the mean particle velocity at different wall-normal positions of the Couette, and figure 15 shows the concentration profile. It is found that the variation in the concentration and mean velocity is much smaller when the collision time is small compared with the viscous relaxation time. This is because the fluctuations generated by inter-particle collisions transport mass and momentum across the flow, thus homogenizing the concentration and mean velocity fields. We also find that there is substantial slip at the wall of the Couette, and the mean particle velocity is different from the velocity of the top plate. There is, once again, quantitative

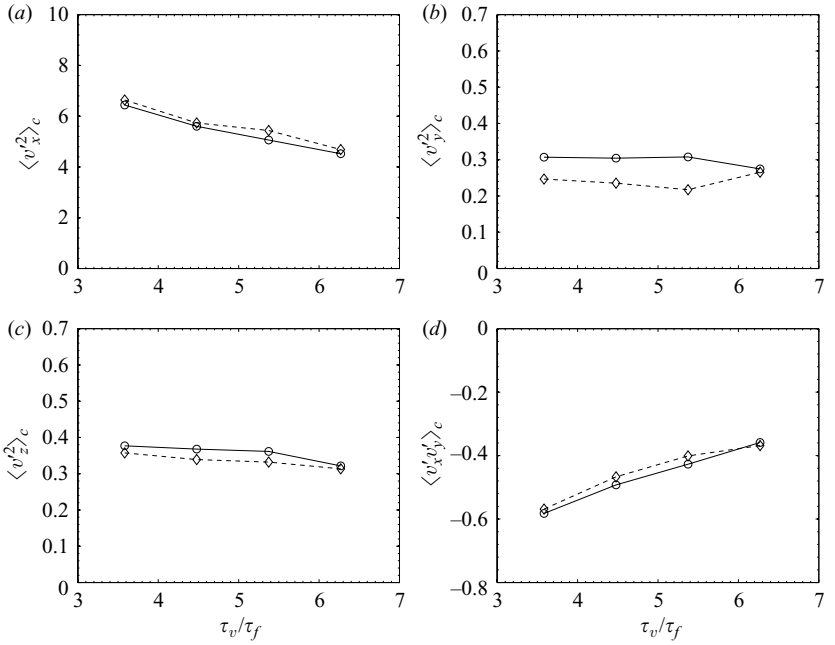

FIGURE 12. The second moments of the particle velocity distribution (*a*) $\langle v_x'^2\rangle$, (*b*) $\langle v_y'^2\rangle$, (*c*) $\langle v_z'^2\rangle$ and (*d*) $\langle v_x'v_y'\rangle$ obtained from the DNS (– – □) and the FFS (—○), averaged over the central 20 % of the Couette. The viscous relaxation time of the particle is less than the particle–wall collision time ($\tau_v < \tau_{c_{pw}}$) and $\phi = 1.9 \times 10^{-5}$. Simulation from run 6 to run 9. The detailed parameters of all the runs are given in table 1.

agreement between the complete DNSs and the fluctuating-force simulation. The ratio of the viscous relaxation time and the integral time scale varies in the range 10–38 for the results shown in figures 14 and 15. Therefore, the assumption of Gaussian white noise for the fluctuating force is a good one in this case. This explains the excellent agreement between the DNS and the fluctuating-force simulations.

Figure 16 shows variation of the mean square of the particle velocities in the three directions and also the second moment of the fluctuating velocity $\langle v_x'v_y'\rangle$ for $\tau_c < \tau_v$. In this case, collisions tend to equalize the root mean square velocities across the channel, and the variations across the channel are much less than those for $\tau_v < \tau_c$. The mean square velocity in the streamwise direction is larger than that in the wall-normal and the spanwise direction by a factor of about two in the centre of the channel, though the streamwise mean square velocity is much larger near the wall. This is due to an increase in the mean square of the fluid velocity fluctuations at the wall, which results in a greater fluctuating force in this region. An interesting observation is that $\langle v_y'^2\rangle$, $\langle v_z'^2\rangle$ and the concentration are nearly uniform across the Couette channel. This implies that the component τ_{yy}^p of the streaming stress tensor for the particle phase is nearly constant across the channel. (Note that at the very low volume fractions under consideration, the collisional stress is negligible in comparison with the streaming stress.) This implies that the net force exerted by the fluid on the particles in the y and z directions is negligible because the gradient of the stress is equal to the net force. The component τ_{xy}^p is found to be non-zero, indicating that there is a local non-zero net force exerted by the fluid on the particles in the x direction. Therefore, the particle velocity fluctuations are driven by the force exerted by the fluid velocity fluctuations in the x direction and the difference between the particle and fluid mean velocities;

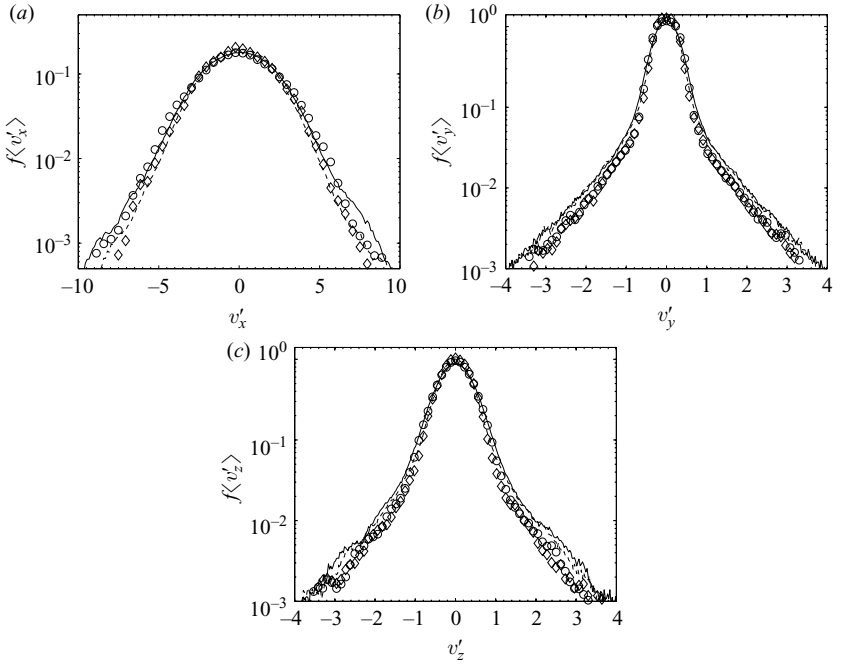

FIGURE 13. Particle velocity distribution function at the centre core of the Couette for the (*a*) streamwise, (*b*) wall-normal and (*c*) spanwise components of velocity fluctuations. The viscous relaxation time of the particle is less than the particle–wall collision time ($\tau_v < \tau_{c_{pw}}$) and $\phi = 1.9 \times 10^{-5}$. Simulation: run 7, DNS (○); run 9, DNS (◇); run 7, FFS (—); run 9, FFS (——). The parameters for all the runs are given in table 1.

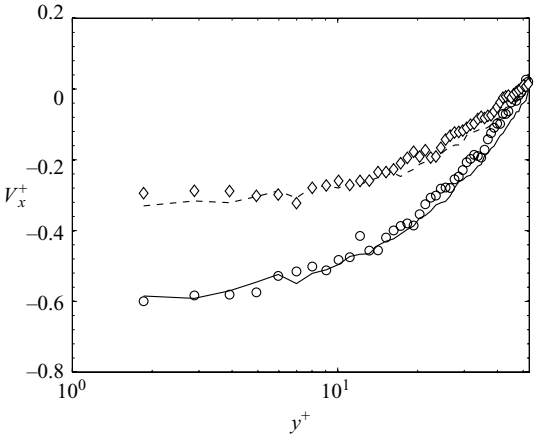

FIGURE 14. Variation of the streamwise particle velocity in the wall-normal direction. The particle–particle collision time is less than the viscous relaxation time of the particle ($\tau_{c_{pp}} < \tau_v$) and $\phi = 7.0 \times 10^{-4}$. Simulation: run 13, DNS (○); run 16, DNS (◇); run 13, FFS (—); run 16, FFS (——). The parameters for all the runs are given in table 1.

this is then transmitted to the cross-stream directions because of collisions. The results of the fluctuating-force simulations are, once again, in quantitative agreement with those of the complete DNSs.

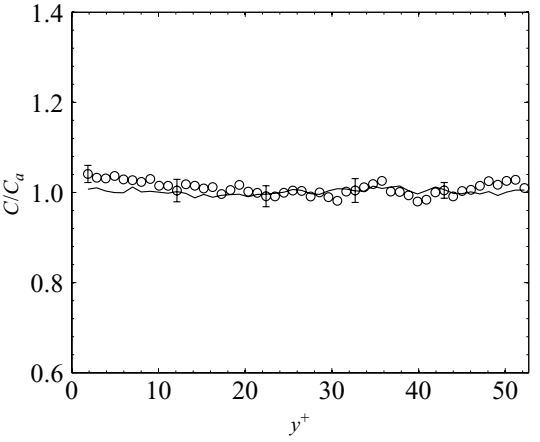

FIGURE 15. Variation of the normalized particle concentration. The particle–particle collision time is less than the viscous relaxation time of the particle ($\tau_{c_{pp}} < \tau_v$) and $\phi = 7.0 \times 10^{-4}$. Simulation: run 13, DNS (○); run 13, FFS (—). The parameters for run 13 are given in table 1.

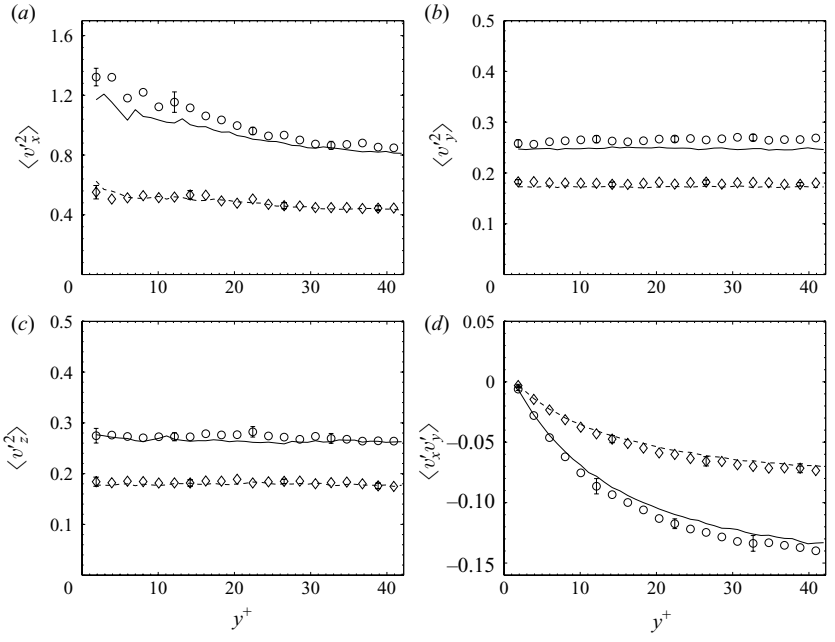

FIGURE 16. Variation of the second moments of the particle velocity distribution (*a*) $\langle v_x'^2 \rangle$, (*b*) $\langle v_y'^2 \rangle$, (*c*) $\langle v_z'^2 \rangle$ and (*d*) $\langle v_x' v_y' \rangle$ at different cross-stream positions. In all the cases particle-particle collision time is less than the viscous relaxation time of the particle ($\tau_{c_{pp}} < \tau_v$) and $\phi = 7.0 \times 10^{-4}$. Simulation: run 13, DNS (○); run 16, DNS (◇); run 13, FFS (—); run 16, FFS (——). The parameters for all the runs are given in table 1.

In figure 17 we show the mean square velocities averaged over the central 20 % of the channel as a function of the ratio of the viscous relaxation time and the integral time scale for the fluid. The agreement between the DNS and the fluctuating-force simulations is excellent, as expected, when the ratio of the viscous relaxation time and the integral time scale is large. Figure 18 shows the distribution functions for the

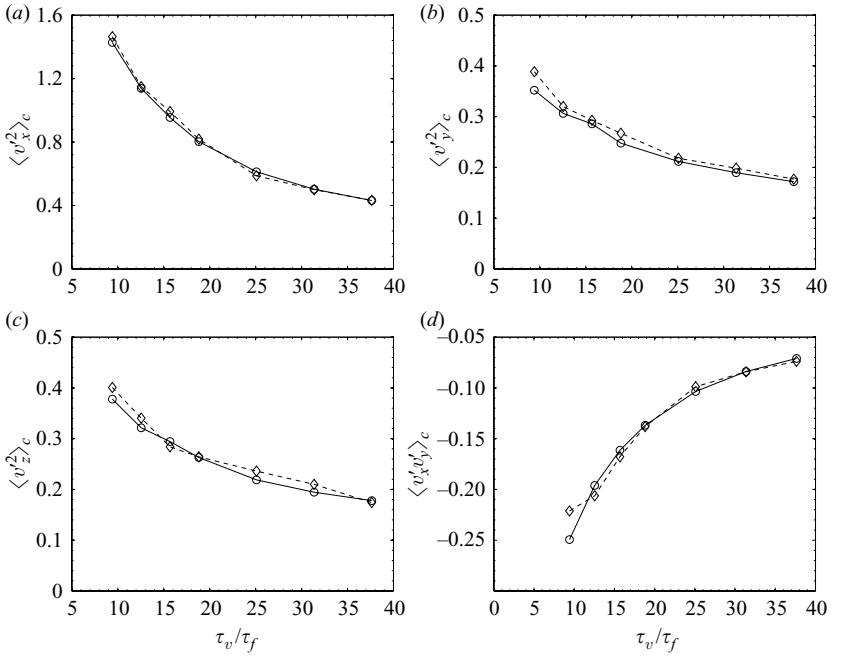

FIGURE 17. The second moments of the particle velocity distribution (*a*) $\langle v_x'^2\rangle$, (*b*) $\langle v_y'^2\rangle$, (*c*) $\langle v_z'^2\rangle$ and (*d*) $\langle v_x'v_y'\rangle$ obtained from the DNS (— — ⋄) and the FFS (—○), averaged over the homogeneous centre core of the Couette. The Particle–particle collision time is less than the viscous relaxation time of the particle ($\tau_{c_{pp}} < \tau_v$) and $\phi = 7.0 \times 10^{-4}$. Simulation: run 10 to run 16. The parameters for all the runs are given in table 1.

fluctuating velocities in the three directions. As expected, the particle velocity distribution function is well approximated by a Gaussian distribution in all cases, and the root mean square velocities in the three directions differ by only about 25 %. (We have not potted the corresponding Gaussian fits for clarity.) The fluctuating-force simulation captures, quantitatively, the probability distribution function for the velocities in all three directions, even when the value of the distribution function is as small as 10^{-3}.

Finally, we address the issue of the extent of change in the particle velocity fluctuations because of the gas turbulence, especially when the viscous relaxation time is large so that the particle inertia is large. In this regime, fluctuations could be generated in two ways: the first is due to the particle mean velocity variation across the channel which generates collisions, and the second is due to turbulent velocity fluctuations. It is of interest to examine what fraction of the particle velocity fluctuations is actually induced by the fluid turbulence. To do this, we carry out simulations for the same system with and without turbulent fluctuations for a wide range of τ_v and for the two cases: the first one is when $\tau_v < \tau_c$, and the second one is the regime in which $\tau_c < \tau_v$. To quantify the effect of turbulence, across the channel we calculated the factor F defined as

$$F = \left[\frac{\displaystyle\int_0^{2\delta} \left(\langle v_{i_t}'^2 \rangle - \langle v_{i_0}'^2 \rangle \right)^2 \mathrm{d}y}{\displaystyle\int_0^{2\delta} \left(\langle v_{i_t}^2 \rangle \right)^2 \mathrm{d}y} \right]^{1/2}, \tag{4.1}$$

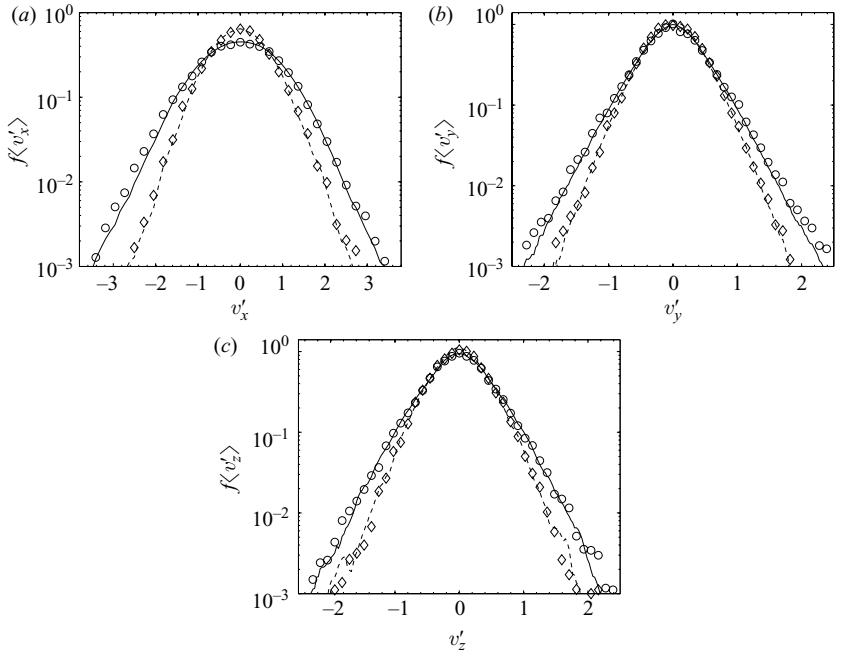

FIGURE 18. The particle velocity distribution function at the centre core of the Couette for the (*a*) streamwise, (*b*) wall-normal and (*c*) spanwise components of velocity fluctuations. The particle–particle collision time is less than the viscous relaxation time of the particle ($\tau_{c_{pp}} < \tau_v$) and $\phi = 7.0 \times 10^{-4}$. Simulation: run 13, DNS (○); run 16, DNS (◇); run 13, FFS (—); run 16, FFS (——). The parameters for all the runs are given in table 1.

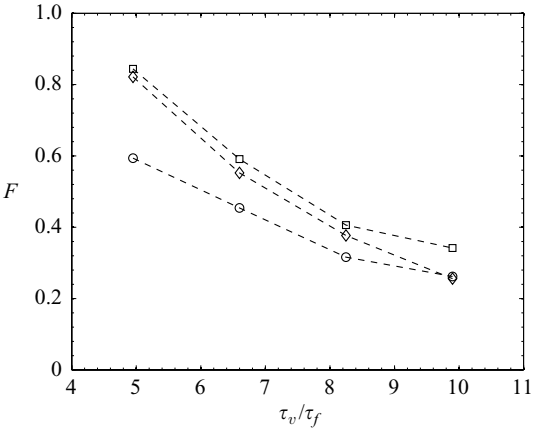

FIGURE 19. Effect of turbulence fluctuation on the second moment of the particle velocity fluctuation, when the viscous relaxation time of the particle is less than the particle–particle collision time ($\tau_v < \tau_{c_{pp}}$) and $\phi = 9.44 \times 10^{-5}$. The streamwise component (— — ○), the wall-normal component (— — ◇) and the spanwise component (— — □); F is defined in (4.1). All the parameters corresponding to the Stokes numbers (τ_v/τ_f) are given in table 1.

where $\langle v_{i_t}'^2\rangle$ is the second moment of the particle velocity fluctuations in presence of turbulence fluctuation and $\langle v_{i_0}'^2\rangle$ is the second moment of the particle velocity in the absence of turbulence fluctuation. Figures 19 and 20 show the decrease in the particle

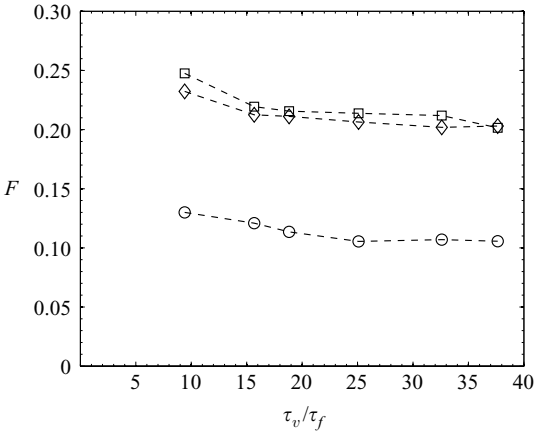

FIGURE 20. Effect of turbulence fluctuation on the second moment of the particle velocity fluctuation, when the particle–particle collision time is less than the viscous relaxation time of the particle ($\tau_c < \tau_v$) and $\phi = 7.0 \times 10^{-4}$. The streamwise component ($- - \bigcirc$), the wall-normal component ($- - \diamond$) and the spanwise component ($- - \square$); F is defined in (4.1). All the parameters corresponding to the Stokes numbers (τ_v/τ_f) are given in table 1.

mean square velocities in the three directions with and without the fluctuating force on the particles for $\tau_v < \tau_c$ and $\tau_c < \tau_v$ respectively. It is observed that the fluctuating force changes the profile of the mean square velocities, resulting in a variation of about 30–80 % for the first case depending on the Stokes number of the particle and 10–25 % for the second case.

The particle velocity fluctuations are generated because of collisions, turbulence and the particle motion across streamlines in the presence of a mean shear. When a particle moves in the cross-stream direction, the mean velocity at the new location is different from that at the old location, but the particle velocity has not changed; so this generates a particle velocity fluctuation in the streamwise direction. In the cross-stream and spanwise directions, the particle velocity fluctuations are generated only because of the turbulent fluctuations and particle collisions. Since the generation of the streamwise particle velocity fluctuations because of the cross-stream motion of particle is present even in the absence of turbulence, the percentage change in the streamwise mean square velocity is lower than that in the cross-stream and spanwise directions. (Note that figures 19 and 20 give the percentage change, and not the absolute change, in the mean square velocities in accordance with (4.1).) In the limit where the collision time is smaller than the viscous relaxation time, there is a greater generation of the particle velocity fluctuations because of collisions owing to the higher frequency of collisions. When the viscous relaxation time is smaller than the collision time, fluctuations in the cross-stream and spanwise directions are generated mainly because of fluid velocity fluctuations. Because of this, the percentage change in the mean square velocity in (4.1) is larger when the viscous relaxation time is small compared with the collision time (figure 19) and is smaller when the collision time is small compared with the viscous relaxation time (figure 20).

5. Theoretical analysis of particle velocity distribution

In this section we present the theoretical analysis of the particle velocity distribution function in two regimes.

d	τ_v	St_γ	$(\tau_v \boldsymbol{D}_{xx})$	$(\tau_v \boldsymbol{D}_{yy})$	$(\tau_v \boldsymbol{D}_{yy}) St_\gamma^2$	$(\dot{\gamma} d)^2$	$\phi(\dot{\gamma} d)^2 St_\gamma^3$
	223.2	10.06	0.85	0.12	12.32	3.85×10^{-3}	3.69×10^{-4}
	267.8	10.70	0.71	0.10	11.63	3.02×10^{-3}	3.50×10^{-4}
1.377	357.1	10.79	0.53	0.08	8.88	1.71×10^{-3}	2.02×10^{-4}
	446.4	11.02	0.43	0.06	7.40	1.16×10^{-3}	1.47×10^{-4}
	535.7	12.26	0.35	0.05	7.62	0.99×10^{-3}	1.72×10^{-4}

TABLE 2. Expected magnitudes of the streamwise mean square velocity because of different sources of the streamwise particle velocity fluctuations.

5.1. *Viscous relaxation time less than collision time*

In the plane Couette flow, the turbulent velocity fluctuations are highly anisotropic, and the fluctuations in the streamwise direction are much larger than that in the wall-normal and spanwise directions. Therefore, one would expect the streamwise particle velocity fluctuations also to be larger than those in the other two directions. The streamwise velocity fluctuations could occur because of three reasons:

(*a*) One would, intuitively, expect the streamwise (x) component of the particle mean square velocity to scale as $(\boldsymbol{D}_{xx}\tau_v)$, owing to the fluctuating force exerted by the fluid turbulent velocity fluctuations in this direction.

(*b*) Another mechanism which could generate streamwise velocity fluctuations is the transport of particles across streamlines because of the cross-stream (y) turbulent velocity fluctuations. The magnitude of the velocity fluctuation in the cross-stream direction is $(\boldsymbol{D}_{yy}\tau_v)^{1/2}$, and this fluctuation transports the particle a distance $(\boldsymbol{D}_{yy}\tau_v)^{1/2} \times \tau_v$ in the cross-stream direction. The streamwise mean square velocity difference because of the cross-stream transport is $(\boldsymbol{D}_{yy}\tau_v)(\dot{\gamma}\tau_v)^2 \sim St_\gamma^2(\boldsymbol{D}_{yy}\tau_v)$, where $St_\gamma = (\dot{\gamma}\tau_v)$ is the Stokes number based on the mean strain rate. Therefore, the streamwise velocity fluctuation because of cross-stream motion scales as $St_\gamma^2 \boldsymbol{T}_{yy}$, where $\boldsymbol{T}_{yy} = (\boldsymbol{D}_{yy}\tau_v)$ is the temperature for the cross-stream velocity fluctuations. We have done simulations in the current paper where the streamwise fluid velocity fluctuations have been switched off, and there are only cross-stream fluid velocity fluctuations. These simulations have verified the scaling $\boldsymbol{T}_{xx} \sim (\boldsymbol{D}_{yy}\tau_v)St_\gamma^2$.

(*c*) A third mechanism is due to the particle collisions induced by the mean velocity gradient of the particle phase. The frequency of such collisions is proportional to $(nd^2(\dot{\gamma} d))$, where $\dot{\gamma}$ is the mean velocity gradient for the particle phase; d is the particle diameter; $(\dot{\gamma} d)$ is the velocity difference between particles on streamlines separated by one particle diameter; and n is the number density of the particles. When expressed in terms of the volume fraction $\phi \sim nd^3$, the collision frequency is $\phi\dot{\gamma}$. The transverse velocity fluctuation induced because of this collision is proportional to $(\dot{\gamma} d)$, and so the particle travels a distance $(\dot{\gamma} d\tau_v)$ in the cross-stream direction because of the collision. The mean square of the velocity fluctuation because of the difference in the mean velocity at these two locations is $\phi(\dot{\gamma} d)^2 St_\gamma^3$.

The expected velocity fluctuations because of these three mechanisms are shown in table 2. It is clear that the dominant contributions are from the fluid turbulent velocity fluctuations in the streamwise direction, as well as because of the fluid turbulent velocity fluctuations in the cross-stream direction inducing the streamwise particle velocity fluctuations. The second mechanism listed above is verified by carrying out simulations in which the streamwise turbulent velocity fluctuations are switched off, and only the cross-stream turbulent fluctuations are incorporated. When both

d	τ_v	St_γ	$(\tau_v \boldsymbol{D}_{yy})$	$(\dot{\gamma} d)^2$	$\phi(\dot{\gamma} d)^2 St_\gamma$	$\boldsymbol{T}_{xx}$	$\phi(\boldsymbol{T}_{xx}^{1/2}\tau_v/d)\boldsymbol{T}_{xx}$
	223.2	10.06	0.12	3.85×10^{-3}	3.65×10^{-6}	4.30	0.136
	267.8	10.70	0.10	3.02×10^{-3}	3.06×10^{-6}	3.83	0.138
1.377	357.1	10.79	0.08	1.71×10^{-3}	1.74×10^{-6}	3.22	0.142
	446.4	11.02	0.06	1.16×10^{-3}	1.20×10^{-6}	2.72	0.137
	535.7	12.26	0.05	0.99×10^{-3}	1.15×10^{-6}	2.38	0.135

TABLE 3. Expected magnitudes of the cross-stream mean square velocity because of different sources of the wall-normal particle velocity fluctuations.

components of the fluid velocity fluctuations are present, it is shown that the total particle mean square velocity is obtained by adding up the contributions because of the two components.

Next, we analyse the cross-stream velocity fluctuations in the limit where the viscous relaxation time is small compared with the time between collisions. The cross-stream particle velocity fluctuations could be due to three reasons:

(*a*) Cross-stream fluid velocity fluctuations.

(*b*) Collisions between particles travelling on nearby streamlines because of the difference in mean velocity, which was the mechanism analysed by Tsao & Koch (1995). The post-collisional cross-stream velocity is $O(d\dot{\gamma})$, and so one would expect the particle velocity fluctuations generated by this mechanism to be $O(d\dot{\gamma})$. The frequency of collisions because of this mechanism is $O((nd^2)(d\dot{\gamma}))$, where n is the number of particles per unit volume. Therefore, the rate of increase in the fluctuating velocity because of collisions is $O((nd^2)(d\dot{\gamma})^3) \sim \phi(d\dot{\gamma})^2\dot{\gamma}$. The rate of decrease in the mean square of the cross-stream fluctuations is $O(\boldsymbol{T}_{yy}/\tau_v)$, where $\boldsymbol{T}_{yy}$ (the cross-stream granular temperature) is the mean square of the cross-stream velocity fluctuations. From this, we find that the granular temperature $\boldsymbol{T}_{yy} \sim \phi(d\dot{\gamma})^2 St_\gamma$, where the Stokes number $St_\gamma = (\dot{\gamma}\tau_v)$.

(*c*) The third mechanism for the generation of cross-stream fluctuations is the collisions induced by the streamwise velocity fluctuations. If $\boldsymbol{T}_{xx}$ is the mean square of the streamwise velocity fluctuations (granular temperature in the streamwise direction), then the frequency of collisions because of this mechanism is $(nd^2\boldsymbol{T}_{xx}^{1/2})$. The post-collisional cross-stream velocity because of this mechanism is $O(\sqrt{\boldsymbol{T}_{xx}})$, and so the rate of increase of the cross-stream fluctuations owing to this mechanism is $O(nd^2\boldsymbol{T}_{xx}^{3/2})$. The rate of decrease of the cross-stream velocity fluctuations because of viscous drag is $O(\boldsymbol{T}_{yy}/\tau_v)$. A balance between these indicates that $\boldsymbol{T}_{yy} \sim (nd^2\boldsymbol{T}_{xx}^{1/2}\tau_v)\boldsymbol{T}_{xx} \sim \phi(\sqrt{\boldsymbol{T}_{xx}}\tau_v/d)\boldsymbol{T}_{xx}$.

The magnitudes of the particle velocity fluctuations because of these three mechanisms, as well as the mean square velocities, are shown in table 3.

It is clear, from table 3, that the cross-stream particle velocity fluctuations because of the second mechanism above (difference in mean velocity on nearby streamlines) is smaller than that because of the first and third mechanisms. The third mechanism (collisions between particles induced to the streamwise particle velocity fluctuations) results in a relatively small mean square velocity because the source of fluctuations is proportional to the volume fraction, which is small. However, the magnitude of the post-collisional velocity because of this mechanism is larger than that because of the first mechanism, which is the cross-stream turbulent velocity fluctuations. Therefore, we would expect the third mechanism to be dominant at larger velocities corresponding to the non-Gaussian high-velocity tails of the distribution functions.

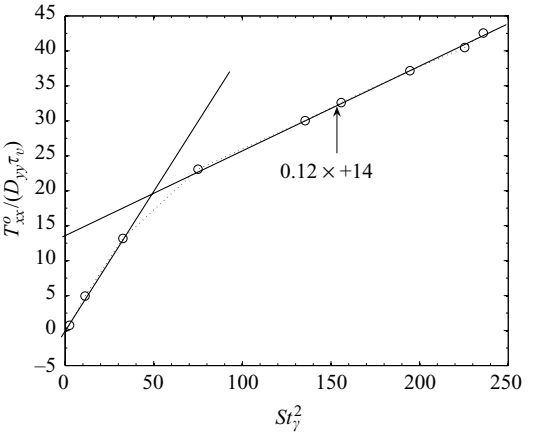

FIGURE 21. The particle velocity fluctuation in the streamwise direction in the presence of mean shear and the cross-stream fluid velocity fluctuation but in the absence of the streamwise fluid velocity fluctuation, when the viscous relaxation time of the particle is less than the particle–particle collision time ($\tau_v < \tau_{c_{pp}}$) and $\phi = 9.44 \times 10^{-5}$.

In the analysis, we derive the cross-stream velocity distributions generated because of collisions between particles induced by the streamwise velocity fluctuations, and verify that the high-velocity tails of the distribution function can be predicted by this mechanism.

The streamwise velocity distribution is first analysed in the limit where the particle relaxation time is less than the collision time. This expected scaling is tested in the fluctuating-force simulations in the centre of the Couette flow by setting $\boldsymbol{D}_{xx} = 0$, while the other two components of the diffusivity and the mean strain rate are non-zero. The Stokes number in the simulations is changed by changing the mass density of the particle while keeping the flow velocity a constant, which in turn changes the viscous relaxation time of the particles. The results for $(\boldsymbol{T}_{xx}/(\boldsymbol{D}_{yy}\tau_v))$ versus St^2_γ, shown in figure 21, show two linear regimes, both of which intersect at a Stokes number (based on the local strain rate) of about 7. The linear fit at low Stokes number passes through the origin, as expected, because the streamwise velocity fluctuations should become zero when the strain rate is zero. The linear fit at high Stokes number, which is of primary interest in the present analysis, does have a non-zero intercept at zero Stokes number. The reason for the transition between the two regimes is not clear at present and needs to be studied further.

Next, we consider the situation in which the streamwise particle velocity fluctuations are induced because of both the streamwise diffusivity $\boldsymbol{D}_{xx}$ in the Boltzmann equation (2.1) and the particle motion across streamlines owing to the cross-stream turbulent fluctuations. In this case, our simulations show (figure 22) that the two contributions are additive, that is to say $\boldsymbol{T}_{xx} = (\tau_v \boldsymbol{D}_{xx}) + \tau_v \boldsymbol{D}_{yy}(14 + 0.12St^2_\gamma)$ in the high-Stokes-number regime. Therefore, the streamwise mean square velocity $\boldsymbol{T}_{xx}$ is the sum of the contributions because of the streamwise diffusivity $\boldsymbol{D}_{xx}$ and the particle motion across the streamlines because of the cross-stream diffusivity $\boldsymbol{D}_{yy}$.

The distribution function for the cross-stream velocities induced by the streamwise velocity fluctuations can be calculated as follows. In this calculation, we assume that collisions are induced by the velocity difference between particles with velocity in the streamwise direction, since the cross-stream velocity fluctuations are small compared

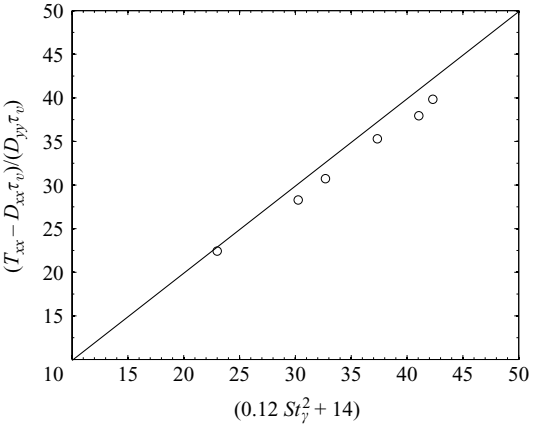

FIGURE 22. Scaling for the streamwise velocity fluctuation in presence of shear and the streamwise fluid velocity fluctuation to depict the contribution of the two sources, when the viscous relaxation time of the particle is less than the particle–particle collision time ($\tau_v < \tau_{c_{pp}}$) and $\phi = 9.44 \times 10^{-5}$.

with those in the streamwise direction. The viscous relaxation time is considered to be small compared with the time between collisions. The pre-collisional distribution function for the particles is of the form

$$f = \frac{1}{\sqrt{2\pi \boldsymbol{T}_{xx}}} \exp\left(-v_x^2/2\boldsymbol{T}_{xx}\right)\delta(v_y)\delta(v_z). \tag{5.1}$$

Since the collisional probability has cylindrical symmetry about the x axis for particles with velocity fluctuations in the x direction, it is most convenient to consider a cylindrical coordinate system with velocity components v_x and $v_r = \sqrt{v_y^2 + v_z^2}$ and meridional angle $\phi = \arctan(v_z/v_y)$.

The distribution function for the radial velocity of the particles, v_r, is calculated from the Boltzmann equation. Since we have neglected the fluctuating force in the radial direction, the dominant terms in the Boltzmann equation are the acceleration because of the fluid drag, i.e. $-(v_r/\tau_v)$, and the collision integral. If $N_{in}(v_r)v_r\mathrm{d}v_r\mathrm{d}\phi$ and $N_{out}(v_r)v_r\mathrm{d}v_r\mathrm{d}\phi$ are the fluxes of particles into and out of the differential volume $v_r\mathrm{d}v_r\mathrm{d}\phi$ because of collisions (with dimensions of number of particles per unit time), then the Boltzmann equation can be written as

$$-\frac{1}{\tau_v v_r}\frac{\partial}{\partial v_r}\left(v_r^2 f(v_r)\right) = N_{in}(v_r) - N_{out}(v_r). \tag{5.2}$$

Here, $N_{in}(v_r)$ is the flux of particles into a differential volume because of collisions between particles with pre-collisional velocities $\boldsymbol{v}'$ and $\boldsymbol{v}^{*'}$, such that the radial velocity of one of the particles is in the differential volume $\mathrm{d}v_r$ about v_r. It will be shown, a little later, that v_r is close to zero for most of the particles, and the fraction of particles with $v_r \sim \sqrt{\boldsymbol{T}_{xx}}$ is $O(\tau_v/\tau_c)$, which is small in the limit $\tau_v \ll \tau_c$. Therefore, while calculating the collisional influx of particles, we consider collisions between pairs of particles with velocity distributions given by (5.1).

Consider a collision between two particles with velocities v_x and v_x^*, such that the line joining the centres of the particles makes an angle θ with the x axis. It is convenient to express the particle velocities in terms of the velocity of the centre of

mass v_x and the relative velocity w_x,

$$\hat{v}_x = (v_x + v_x^*)/2, \tag{5.3}$$

$$w_x = v_x - v_x^* \tag{5.4}$$

The velocity of the centre of mass is unchanged in a collision. In an elastic collision between smooth particles, the relative velocity along the line joining the centres of the particles is reversed, while the relative velocity tangential to the surfaces at contact is unchanged. The post-collisional relative velocities w_r' and w_x' are related to the pre-collisional relative velocity w_x by

$$w_r' = w_x \sin(2\theta), \tag{5.5}$$

$$w_x' = -w_x \cos(2\theta). \tag{5.6}$$

The frequency of collisions between the pairs of particles with relative velocity w_x is given by

$$\nu(w_x, \theta, \phi)\, \mathrm{d}w_x \sin(\theta)\, \mathrm{d}\theta\, \mathrm{d}\phi = n^2 f(w_x) d_p^2 (w_x \cos(\theta))\, \mathrm{d}w_x \sin(\theta)\, \mathrm{d}\theta\, \mathrm{d}\phi. \tag{5.7}$$

Here, $(w_x \cos(\theta))$ is the component of the relative velocity along the line joining the centres of the particles, and d_p is the particle diameter. Since the collision results in a pair of particles with post-collisional velocity (w_r', w_x'), the collision frequency can be re-expressed in terms of the post-collisional relative velocity instead of the pre-collisional relative velocity,

$$\nu(w_r', w_x', \phi) w_r'\, \mathrm{d}w_r'\, \mathrm{d}w_x'\, d\phi = n^2 f(w_x)\, d_p^2 (w_x \cos(\theta))\, \mathrm{d}w_x \sin(\theta)\, \mathrm{d}\theta\, \mathrm{d}\phi. \tag{5.8}$$

Using the relations between the pre- and post-collisional relative velocities, (5.5) and (5.6), we obtain the expression for the collision frequency as

$$\nu(w_r', w_x', \phi) = \frac{n^2 f(w_r', w_x') d_p^2}{2\sqrt{w_r'^2 + w_x'^2}}. \tag{5.9}$$

In deriving the above equation, we have used the relationship $\mathrm{d}w_x\, \mathrm{d}\theta = (2\sqrt{w_r'^2 + w_x'^2})^{-1}\, \mathrm{d}w_r'\, \mathrm{d}w_x'$ for the transformation of coordinates, and the distribution function (5.1) can be expressed in terms of (w_r', w_x') as

$$f_w(w_r', w_x') = \frac{1}{\sqrt{4\pi \boldsymbol{T}_{xx}}} \exp\left(- \left(w_x'^2 + w_r'^2\right)/4\boldsymbol{T}_{xx}\right). \tag{5.10}$$

Since we are interested only in the cross-stream velocity of the particles, the collision frequency (5.9) can be integrated over all angles ϕ and the relative streamwise velocities w_x', to obtain

$$\nu(w_r', \phi) = \int \mathrm{d}w_x' \nu(w_r', w_x', \phi) = (1/(8\sqrt{\pi \boldsymbol{T}_{xx}})) n^2 d_p^2 \exp\left(- w_r'^2/8\boldsymbol{T}_{xx}\right) K_0\left(w_r'^2/4\boldsymbol{T}_{xx}\right), \tag{5.11}$$

where K_0 is the modified Bessel function. In the above calculation, we have integrated over the domain $-\infty \leqslant w_x' \leqslant \infty$. The above collision results in a particles with radial velocity $v_r = (w_r'/2)$. Therefore, the flux of particles into the differential volume $\mathrm{d}v_r$ about v_r is

$$N_{in}(v_r, \phi) = (1/(2\sqrt{\pi \boldsymbol{T}_{xx}})) n^2 d_p^2 \exp\left(- v_r^2/2\boldsymbol{T}_{xx}\right) K_0\left(v_r^2/\boldsymbol{T}_{xx}\right). \tag{5.12}$$

The collisional flux of particles out of the differential volume $N_{out}(v_r)$ is due to the collision of particles with velocity in the differential volume v_r with other particles. This collision frequency can be written, using the molecular chaos approximation, as

$$\nu(\boldsymbol{v}) = n^2 \int \mathrm{d}\boldsymbol{k} \int \mathrm{d}\boldsymbol{v}^* f(\boldsymbol{v}) f(\boldsymbol{v}^*) d_p^2 (\boldsymbol{v} - \boldsymbol{v}^*).\boldsymbol{k}, \tag{5.13}$$

where $\boldsymbol{k}$ is the unit vector along the line joining the centres of the particles, and the above integral is carried out over all velocities $\boldsymbol{v}^*$. The above integral is difficult to evaluate analytically, but simplifications can be made when the fraction of particles with radial velocity $v_r \sim \sqrt{\boldsymbol{T}_{xx}}$ is small. In this case, we can assume that the velocity of the second colliding particle, v^*, is given by (5.1); the error made because of this is proportional to the ratio (τ_c/τ_v). In addition, while calculating the integral, we assume that the relative velocity distribution for the particles is given by (5.10). This approximation is a good one if the radial velocity of $v_r \ll \sqrt{\boldsymbol{T}_{xx}}$. It is a poor approximation for particles with radial velocity $v_r \sim \sqrt{\boldsymbol{T}_{xx}}$. However, in the latter case, the dominant mechanism of transport of particles in velocity space is due to the viscous drag; the flux of particles because of collisions is $O(\tau_v/\tau_c)$ smaller than that because of the viscous drag. Therefore, this approximation for the relative velocities provides a uniform approximation for all particles. With this, the collisional flux $N_{out}(v_r)$ is given by

$$N_{out}(v_r) = n d_p^2 \sqrt{\pi \boldsymbol{T}_{xx}}\, f(v_r). \tag{5.14}$$

With the above approximation for $N_{out}(v_r)$, the equation for the radial distribution function becomes

$$\begin{aligned} \frac{\partial f(v_r)}{\partial v_r} + \frac{(2-\epsilon) f}{v_r} &= -\frac{1}{\sqrt{\pi \boldsymbol{T}_{xx}}} \frac{n^2 d_p^2 \tau_v}{v_r} \exp\left(-v_r^2/2\boldsymbol{T}_{xx}\right) K_0(v_r^2/2\boldsymbol{T}_{xx}) \\ &= -\frac{\epsilon}{2\pi \boldsymbol{T}_{xx} v_r} \exp\left(-v_r^2/2\boldsymbol{T}_{xx}\right) K_0\left(v_r^2/2\boldsymbol{T}_{xx}\right), \end{aligned} \tag{5.15}$$

where $\epsilon = (2\tau_v n d_p^2 \sqrt{\pi \boldsymbol{T}_{xx}})$ is proportional to the ratio of the viscous relaxation time and the time between collisions. The above equation can be easily solved to obtain f as a function of v_r,

$$f(v_r) = -\frac{\epsilon}{2\pi \boldsymbol{T}_{xx}} v_r^{\epsilon-2} \int_{\infty}^{v_r} \mathrm{d}v_r' (v_r')^{1-\epsilon} \exp\left(-(v_r')^2/2\boldsymbol{T}_{xx}\right) K_0((v_r')^2/2\boldsymbol{T}_{xx}). \tag{5.16}$$

The integral in (5.15) is difficult to carry out analytically. However, it is easily verified that the above distribution function is normalized, that is

$$\int_0^{2\pi} \mathrm{d}\phi \int_0^{\infty} \mathrm{d}v_r\, v_r f(v_r) = 1. \tag{5.17}$$

The mean square of the radial velocity is easily calculated from the above distribution function (5.16),

$$\begin{aligned} \langle v_r^2 \rangle &= \int_0^{2\pi} \mathrm{d}\phi \int_0^{\infty} \mathrm{d}v_r\, v_r^3 f(v_r) \\ &= \frac{4\boldsymbol{T}_{xx}\epsilon}{3(2+\epsilon)}. \end{aligned} \tag{5.18}$$

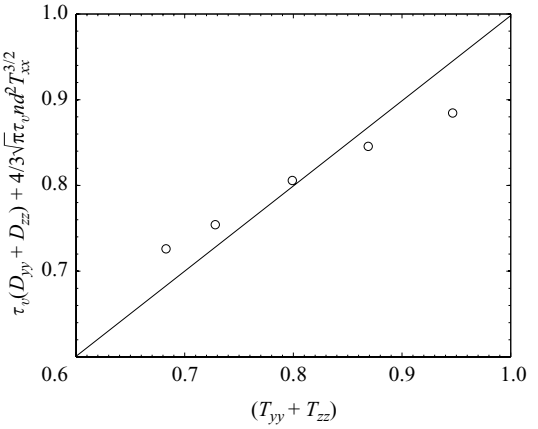

FIGURE 23. The mean square radial velocity of the particle obtained from the theory and simulation, when viscous relaxation time of the particle is less than the particle–particle collision time ($\tau_v < \tau_{c_{pp}}$) and $\phi = 9.44 \times 10^{-5}$.

In the limit $\epsilon \to 0$, the leading approximation for the above equation is

$$\begin{aligned}\langle v_r^2 \rangle &= \frac{2\boldsymbol{T}_{xx}\epsilon}{3} \\ &= \frac{4\sqrt{\pi}\tau_v n \mathrm{d}^2 \boldsymbol{T}_{xx}^{3/2}}{3}.\end{aligned} \tag{5.19}$$

Though an analytical expression for the distribution function is difficult to obtain, the limiting behaviours for $v_r \ll \sqrt{\boldsymbol{T}_{xx}}$ and $v_r \gg \sqrt{\boldsymbol{T}_{xx}}$ are easily obtained. For $v_r \gg \sqrt{\boldsymbol{T}_{xx}}$, the Bessel function $K_0(v_r^2/2\boldsymbol{T}_{xx}) \sim \sqrt{\pi/2(v_r^2/2\boldsymbol{T}_{xx})}\exp(-v_r^2/2\boldsymbol{T}_{xx})$, and so the distribution function

$$f \sim \frac{\Gamma((1-\epsilon)/2, (v_r^2/\boldsymbol{T}_{xx}))}{v_r^{2-\epsilon}}. \tag{5.20}$$

This indicates a rapid decay in the distribution function, faster than an exponential. For $v_r \ll \sqrt{\boldsymbol{T}_{xx}}$, the Bessel function has the asymptotic behaviour $K_0(v_r^2/2\boldsymbol{T}_{xx}) \to -\log(v_r^2/4\boldsymbol{T}_{xx}) - \gamma$. In this case, it is easily verified that

$$f \sim \frac{\log(v_r^2/\boldsymbol{T}_{xx})}{2-\epsilon} \tag{5.21}$$

Equation (5.19) describes the particle radial velocity, originating only from the streamwise fluid velocity fluctuation and as a result of the particle–particle collision. In presence of the spanwise and wall-normal fluid velocity fluctuations we have superimposed the contribution from the streamwise component with that which originates from the other two and compared it with the simulation in figure 23. The theoretical distribution function equation (5.16) is compared with the results of fluctuating-force simulation in figure 24. It is clear that the asymptotic form (5.16) shows a slower decay than the distribution function in the simulations, for two reasons. Firstly, the turbulent diffusion in the cross-stream and spanwise directions are neglected in the derivation of (5.16); this could account for the rapid initial decay in the simulation results in figure 24. Secondly, the ratio of the viscous relaxation time and the particle–wall collision time is only between 2 and 3 in these simulations. Nevertheless, it is clear that the high-velocity decay in the simulations is slower than

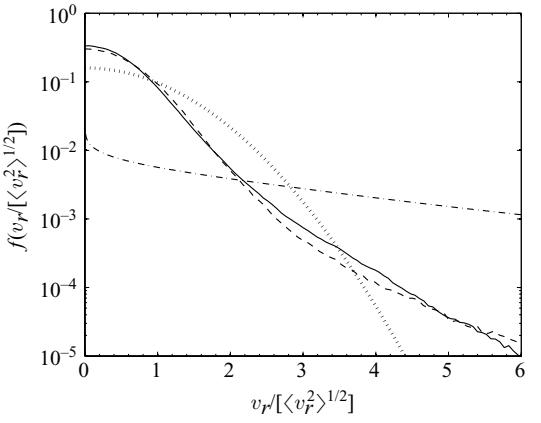

FIGURE 24. The radial velocity distribution of the particle obtained from the simulation and theory. Simulation, ($\tau_v < \tau_{c_{pp}}$), run 1 (—); simulation, ($\tau_v < \tau_{c_{pw}}$), run 7 (——), and theory (—.—) and the Gaussian distribution ($\cdots$). The theoretical results for both the cases are very much similar. The descriptions of run 1 and run 7 are in table 1.

the Gaussian distribution, and the trends in the high-velocity decay are correctly predicted by the theory. Even though the theoretical agreement is not very good, the derivation is exact in the limit in which it was derived, similar to the derivation of Kumaran & Koch (1993*a*) and Tsao & Koch (1995). Such asymptotic calculations of far-from-Gaussian distributions in non-equilibrium systems are rare. In future, we intend to carry out simulations with much larger channel widths, where the viscous relaxation time is much smaller than the collision time, in order to validate the theoretical results.

5.2. *Collision time smaller than the viscous relaxation time*

In the regime in which the particle collision time is small compared with the viscous relaxation time, one might intuitively expect that the collision integral in the Boltzmann equation can be set equal to zero in the leading approximation, and the leading-order distribution function is a Maxwell–Boltzmann distribution. The temperature of the distribution function is set by a balance between the production of energy (because of the turbulent fluid velocity fluctuations or because of mean shear) and the dissipation because of mean drag. The correction to the distribution function because of mean shear has already been evaluated in the standard Chapman–Enskog calculation of the viscosity of a dilute gas, while the correction because of turbulent fluctuations would be given by a simple energy balance equation where the source of fluctuations because of turbulent fluctuations is balanced by the dissipation because of viscous drag. However, the present simulations do not fall in this regime for two reasons:

(*a*) The first is that the time between wall collisions is smaller than that between the particle–particle collisions in runs 10–16 in table 1. This implies that the Knudsen number, which is the ratio of the mean free path and the macroscopic scale, is larger than 1. There have been previous studies of a sheared granular flow in the high-Knudsen-number regime (Kumaran 1997; Kumaran 2006*b*), but the source of shear in these studies is the transfer of momentum from the wall to the particle because of friction. This frictional source is not included in the present analysis, and

τ_v	$n(\boldsymbol{T}_{xy}+\boldsymbol{T}_{yy}+\boldsymbol{T}_{zz})/3$	$\tau_v(\boldsymbol{D}_{xy}+\boldsymbol{D}_{yy}+\boldsymbol{D}_{zz})/3$	$\boldsymbol{T}_{xy}$	$\tau_v\boldsymbol{D}_{xy}$
509.3	0.719	0.164	−0.249	−0.093
679.0	0.589	0.123	−0.196	−0.070
848.8	0.512	0.098	−0.161	−0.056
1018.5	0.438	0.082	−0.137	−0.047
1358.0	0.348	0.061	−0.104	−0.035
1697.5	0.296	0.047	−0.084	−0.027
2037.0	0.260	0.041	−0.071	−0.023

TABLE 4. The second moment of the particle velocity fluctuation (particle temperature) obtained from the simulation and estimated from the fluid phase velocity fluctuation.

so the results are not directly comparable with studies on granular materials in the Knudsen regime. However, a common result for both smooth and rough particles is that the standard expression for the strain rate of a dilute low-Knudsen-number gas significantly overestimates the stress in the high-Knudsen-number regime. The ratio of the actual stress and the stress obtained from Newton's law of viscosity in the high-Knudsen-number limit scales as $(\phi L/d)^3 \log(\phi L/d)$ for smooth particles, whereas it depends on the details of the collision law for rough particles. In our analysis, this ratio is small, in the range 10^{-5}–10^{-6}.

(*b*) In addition, Newton's law for viscosity will be valid only when the particle fluctuating velocity is large compared with the product of the strain rate and the mean free path. In our simulations, we find that $(\dot{\gamma}\lambda/T^{1/2}) \sim (\dot{\gamma}d/\phi T^{1/2})$ is typically large, with a value in the range 10–100. Therefore, the motion of the particles is not similar to that in a dilute gas of molecules.

Further work needs to be carried out to model the stress in the high-Knudsen-number regime with turbulent velocity fluctuations.

In table 4 we examine whether the turbulent fluctuations could induce the particle velocity fluctuations in the centre of the channel. It is clear that the expected mean square velocity because of fluid turbulent fluctuations is smaller than the actual mean square velocity, though they differ only by a factor between two and five. Therefore, it is clear that the turbulent fluctuations in the centre region of the channel alone are not sufficient to account for the particle velocity fluctuations. It is possible that the larger value of the particle velocity fluctuations could be due to the transport of particles across the channel and the higher turbulent velocity fluctuations near the wall in the high-Knudsen-number regime. However, the turbulent diffusion model does give the correct magnitude of the particle mean square velocities.

6. Summary and conclusion

A Langevin model has been formulated for including the effect of turbulent velocity fluctuations on the particles in a turbulent gas–solid suspension, in the regime in which the viscous relaxation time of the particles and the time between collisions are large compared with the integral time scale for the fluid velocity fluctuations. Advantage has been taken of the time scale separation to treat the effect of turbulent velocity fluctuations as a Gaussian random noise acting on the particle phase, in addition to the drag force exerted because of the difference between the particle velocity and the fluid mean velocity. The analysis of the DNS of a turbulent gas–solid suspension in part 1 of the current paper (Goswami & Kumaran 2010) showed that the probability distribution for the acceleration on the particles is a Gaussian distribution, even when

the probability distribution for the particle velocity is not a Gaussian. In addition, the acceleration distribution was calculated in two ways: the first was to calculate the acceleration distribution function on the particles, and the second was to calculate the acceleration distribution from the distribution of the fluid fluctuating velocity in the absence of the particles. The two were found to be in quantitative agreement. This motivated the present modelling effort, where we have imposed a fluctuating force in a particle simulation to represent the effect of the turbulence. The force is assumed to be a Gaussian white noise which is anisotropic and spatially varying. The second moment of the force is determined from the fluid velocity fluctuations in a direct simulation without particles. The results of this simulation were compared with the result of a complete DNS.

The comparison shows, clearly, that the fluctuating-force model is a good model for representing the turbulent fluctuations, provided the particle viscous relaxation time is greater than about five times the fluid integral time. There is quantitative agreement for the concentration and mean velocity profiles, as well as for the variation of the mean square velocities across the channel. The fluctuating-force model also correctly predicts the velocity distribution function of the particles, even in cases in which the distribution function is very different from a Gaussian distribution. We find that the fluctuating-force model is in error when the viscous relaxation time of the particles is less than about five times the integral time scale. However, when (τ_v/τ_f) is greater than about 5, we are able to obtain quantitative agreement between the fluctuating-force model and complete DNSs. It should be noted that the second moment of the fluctuating force used here is a function of the cross-stream direction, in contrast with the usual Brownian models which assume a uniform fluctuating force. Using this inhomogeneous fluctuation force, we were able to capture the variation of all dynamical quantities up to the wall of the channel, in addition to the mean square velocity fluctuations in the central region of the channel, where the fluid mean square velocities are nearly a constant. Thus, this is a promising method for including the fluid turbulent velocity fluctuations in a particle simulation even when the flow is inhomogeneous and spatially varying.

It should be noted that all of the above results have been obtained for the very limited case in which there is no effect of the particles on the turbulent flow (one-way coupling). This was done as a first step, before focusing the more complicated problem of two-way coupling, where the particles exert a force on the fluid. Future work will focus on carrying out a similar study for the problem with two-way coupling and will examine whether the acceleration distribution can be well represented as a Gaussian random noise in that case as well. In addition, the variation in the mean square velocities across the channel in a Couette flow is lower than that in flows of practical interest, such as the pressure-driven flow in a channel. In the latter case, there is a large variation in the streamwise mean square velocity of the fluid across the channel, and it is of interest to examine whether the present model works for situations with large spatial variations in the fluid velocity fluctuations.

The magnitudes of the velocity fluctuations generated in the centre of the Couette were analysed in detail. In the limit in which the viscous relaxation time is small compared with the time between collisions, the streamwise velocity distribution is still found to be a Gaussian, but the cross-stream distributions contain long tails. We examined three mechanisms for the generation of the streamwise velocity fluctuations in this limit. The particle mean square velocity because of the turbulent fluctuations in the streamwise direction scaled as $\boldsymbol{D}_{xx}\tau_v$. A second mechanism for the generation of streamwise fluctuations was the cross-stream turbulent fluid velocity fluctuations

resulting in the particles moving across streamlines. Since the mean particle velocity varies with position, the cross-stream motion of the particles generates a fluctuating velocity in the streamwise direction. The mean square velocity because of this mechanism was found to be $O(\boldsymbol{D}_{yy}\tau_v St_\gamma^2$, where $St_\gamma = \tau_v\dot{\gamma}$ is the Stokes number based on the mean strain rate and the particle relaxation time. A third mechanism was the collisions between particles on adjacent streamlines moving with mean velocities of $O(d\dot{\gamma})$, where d is the particle diameter. The mean square velocity because of this mechanism is $O(\phi St_\gamma^3(d\dot{\gamma})^2)$. By evaluating the magnitudes of the expected velocity from these three mechanisms, it was found that the contribution because of the collisions between particles on adjacent streamlines is small compared with the other two mechanisms. The mean square velocity is well predicted by a linear combination of the velocities because of streamwise and cross-stream diffusion.

The mechanisms for the generation of the particle velocity fluctuations in the cross-stream direction was also examined. One mechanism is the cross-stream fluid velocity fluctuations, and the mean square fluid velocity fluctuations because of this is $O(\boldsymbol{D}_{yy}\tau_v)$. The second is due to collisions between particles travelling on nearby streamlines because of the difference in mean velocity. The post-collisional cross-stream velocity in a collision is $O(d\dot{\gamma})$, and the mean square velocity in the cross-stream direction because of this mechanism is $O(\phi(d\dot{\gamma})^2 St_\gamma)$. The third mechanism is collisions induced by the streamwise velocity fluctuations. The post-collision velocity generated because of this mechanism is $O(\sqrt{\boldsymbol{T}_{xx}})$, where $\boldsymbol{T}_{xx}$ is the mean square velocity in the streamwise direction, and the mean square velocity owing to this mechanism scales as $O(nd^2\boldsymbol{T}_{xx}^{1/2}\tau_v)\boldsymbol{T}_{xx} \sim \phi(\sqrt{\boldsymbol{T}_{xx}}\tau_v/d)\boldsymbol{T}_{xx}$. By examining these three mechanisms, it was found that the collisions because of the streamwise velocity fluctuations result in the high-velocity tails in the cross-stream velocity fluctuations, while the low-velocity fluctuations are due to the cross-stream turbulent velocity fluctuations. The distribution function for the cross-stream velocity because of collisions induced by the streamwise velocity fluctuations was derived analytically, and the results showed a slow decay of the velocity distribution function at high velocities, in qualitative agreement with the simulation results.

When the time between collisions is small compared with the viscous relaxation time, the particle velocity fluctuations are expected to be nearly isotropic and well described by Gaussian distributions. However, the Knudsen number is typically larger than 1 in our simulations, and the assumption of local rheology will fail in this limit. It is known that Newton's law for viscosity overestimates the viscous stress in the high-Knudsen-number regime for granular flows. Our results show that the particle velocity fluctuations in the centre of the channel are larger than what would be expected if the particles were driven by the turbulent velocity fluctuations alone. This could be because of the motion of particles across the channel, because the fluctuations are larger near the wall than at the centre of the channel.

The authors would like to thank the Department of Science and Technology, Government of India, for financial support.

REFERENCES

Chapman, S. & Cowling, T. G. 1970 *The Mathematical Theory of Non-Uniform Gases*. Cambridge University Press.

Goldhirsch, I. 2003 Rapid granular flows. *Annu. Rev. Fluid Mech.* **35**, 267–293.

Goswami, P. S. & Kumaran, V. 2010 Particle dynamics in a turbulent particle–gas suspension at high stokes number. Part 1. Velocity and acceleration distributions. *J. Fluid Mech.* **646**, 59–90.

Jenkins, J. T. & Richman, M. W. 1985 Grad's 13-moment system for a dense gas of inelastic spheres. *Arch. Rat. Mech. Anal.* **87**, 355–377.

Jenkins, J. T. & Savage, S. B. 1983 A theory for the rapid flow of identical, smooth, nearly elastic particles. *J. Fluid Mech.* **130**, 186–202.

Koch, D. L. 1990 Kinetic theory for a monodisperse gas–solid suspension. *Phys. Fluids* A **10**, 1711–1723.

Kumaran, V. 1997 Velocity distribution function for a dilute granular material in shear flow. *J. Fluid Mech.* **340**, 319–341.

Kumaran, V. 1998*a* Kinetic theory for a vibro-fluidized bed. *J. Fluid Mech.* **364**, 163–185.

Kumaran, V. 1998*b* Temperature of a granular material "fluidised" by external vibrations. *Phys. Rev.* E **57**, 5660–5664.

Kumaran, V. 2003 Stability of a sheared particle suspension. *Phys. Fluids* **15**, 3625–3637.

Kumaran, V. 2004 Constitutive relations and linear stability of a sheared granular flow. *J. Fluid Mech.* **506**, 1–43.

Kumaran, V. 2006*a* The constitutive relations for the granular flow of rough particles, and its application to the flow down an inclined plane. *J. Fluid Mech.* **561**, 1–42.

Kumaran, V. 2006*b* Granular flow of rough particles in the high-Knudsen-number limit. *J. Fluid Mech.* **561**, 43–72.

Kumaran, V. 2008 Dense granular flow down an inclined plane: from kinetic theory to granular dynamics. *J. Fluid Mech.* **599**, 121–168.

Kumaran, V. & Koch, D. L. 1993*a* Properties of a bidisperse particle–gas suspension. Part 1. Collision time small compared to viscous relaxation time. *J. Fluid Mech.* **247**, 623–642.

Kumaran, V. & Koch, D. L. 1993*b* Properties of a bidisperse particle–gas suspension. Part 2. Viscous relaxation time small compared to collision relaxation time. *J. Fluid Mech.* **247**, 643–660.

Louge, M. Y., Mastorakos, E. & Jenkins, J. T. 1991 The role of particle collisions in pneumatic transport. *J. Fluid Mech.* **231**, 345–359.

Lun, C. K. K., Savage, S. V., Jeffrey, D. J. & Chepurniy, N. 1984 Kinetic theories for granular flow: inelastic particles in Couette flow and slightly inelastic particles in a general flow field. *J. Fluid Mech.* **140**, 223–256.

Savage, S. B. & Jeffrey, D. J. 1981 The stress tensor in a granular flow at high shear rates. *J. Fluid Mech.* **110**, 255–272.

Sela, N. & Goldhirsch, I. 1998 Hydrodynamic equations for rapid flows of smooth inelastic spheres, to Burnett order. *J. Fluid Mech.* **361**, 41–74.

Sela, N., Goldhirsch, I. & Noskowicz, S. H. 1996 Kinetic theoretical study of a simply sheared two dimensional granular gas to Burnett order. *Phys. Fluids* **8**, 2337.

Tsao, H.-K. & Koch, D. L. 1995 Shear flows of a dilute gas–solid suspension. *J. Fluid Mech.* **296**, 211–245.